

---

# Studying Small Language Models with Susceptibilities

---

Garrett Baker<sup>\*†</sup>    George Wang<sup>\*†</sup>    Jesse Hoogland<sup>\*</sup>    Daniel Mufet<sup>\*</sup>

## Abstract

We develop a *linear response* framework for interpretability that treats a neural network as a Bayesian statistical mechanical system. A small, controlled perturbation of the data distribution, for example shifting the Pile toward GitHub or legal text, induces a first-order change in the posterior expectation of an observable localized on a chosen component of the network. The resulting *susceptibility* can be estimated efficiently with local SGLD samples and factorizes into signed, per-token contributions that serve as attribution scores. Building a set of perturbations (*probes*) yields a response matrix whose low-rank structure separates functional modules such as multigram and induction heads in a 3M-parameter transformer. Susceptibilities link local learning coefficients from singular learning theory with linear-response theory, and quantify how local loss landscape geometry deforms under shifts in the data distribution.

## 1 Introduction

Although we can observe that large neural networks have complex and interesting behavior, we do not understand the *microscopic organization* that gives rise to this behavior. Condensed matter physics offers a well-tested paradigm for uncovering such hidden structure: apply an infinitesimal, well-controlled perturbation and read out the system’s linear response. Using the correspondence between statistical physics and statistical learning theory (Balasubramanian, 1997; LaMont and Wiggins, 2019) and singular learning theory (Watanabe, 2009) we develop such linear responses, or *susceptibilities*, as a mathematical and empirical foundation for interpretability in neural networks.

Given a neural network, the setup consists of two main ingredients:

- **The Perturbation:** We introduce an infinitesimal shift in the data distribution, for example by biasing the training set to contain slightly more code or scientific prose.
- **The Response:** For a chosen subnetwork (e.g. an individual attention head) we measure how this shift alters the expectation value of an observable that is sensitive to changes in the parameters in that subnetwork. The resulting derivative is the susceptibility.

More formally, given some variation  $q_h(x)$  in the data distribution  $q(x)$ , a posterior distribution  $p(w|h)$  over model parameters  $w$  for this data distribution, and an observable  $\phi(w)$ , we consider

$$\langle \phi \rangle_h = \int \phi(w) p(w|h) dw \quad (1)$$

with  $h$  being the degree of perturbation. The *susceptibility* is, up to constants,

$$\chi \propto \frac{\partial}{\partial h} \langle \phi \rangle_h \Big|_{h=0}. \quad (2)$$

In this paper we introduce the mathematical framework of susceptibilities, and explain how to efficiently estimate these quantities with local Stochastic Gradient Langevin Dynamics (SGLD)

---

<sup>\*</sup>Timaues

<sup>†</sup>Equal contribution

. After few iterations of the feedback loop, the measured light profiles shown in Fig. \[fig:cont\] (continuous light patterns) and Fig. \[fig:disc\] (discrete spot patterns) show increased accuracy and more closely resemble their target patterns. A summary of the improvements to these optical traps due to the feedback process, along with the number of iterations required ( $\nu$ ) and the light-usage efficiency ( $\Gamma$ ), can be found in Table \[tab:res\].

Pattern	Before	After	Before	After	$\nu$	$\Gamma$	$\epsilon$
Indented Ring	21.9	6.7	9.8	2.1	8		21.5
Double Well	19.0	5.5	5.5	0.7	10		20.0
3pt Square Lattice	22.0	15.3	3.6	2.3	10		14.8
Ring Lattice	13.7	10.0	2.5	1.1	10		17.5

: Summary of improvements, including error, iterations ( $\nu$ ) and Efficiency ( $\Gamma$ )

! [Continuous patterns optimised by feedback. (a) A ring pattern with a Gaussian radial distribution and a restriction (as in Fig. \[fig:flow\]), showing the measured Signal Region intensity using the initial MRAC-c algorithm (left) and after 8 iterations of feedback optimisation (right), which improve the signal on the left from 9.8% to 2.1%. (Below) The intensity around the circumference of the ring showing the target pattern (red), and the measured profile before (green) and after (blue) feedback. (b) RMS error progression for the ring pattern with restriction, recorded at each step of the feedback algorithm. (c) A Gaussian double-well pattern, showing Signal-Region intensity before (left) and after (right) feedback. (Below) A cut across the centre of the two wells, showing normalised pixel intensity for

Figure 1: Visualizing per-token susceptibilities for three heads on a sample from arxiv. Each token is highlighted in three segments (top, middle, bottom) which correspond to the per-token susceptibilities for three heads (0:0,1:2,1:7). Green means positive susceptibility and red means negative (more solid color means higher magnitude, with zero being white). We see that positive susceptibilities are often associated with word endings and structural elements like brackets ], \$ while negative susceptibilities are associated with spaces and word beginnings.

(Welling and Teh, 2011). We then apply this framework to a small (3M parameter) transformer trained on the Pile (Gao et al., 2020). As our variations of the data distribution, we take mixtures of the training distribution  $q$  with Pile subsets  $q'$  as in  $(1 - h)q + hq'$ . For example, these variations may “dial up” the probability of code (if  $q'$  is github) or legal discourse (if  $q'$  is freelaw).

Further, we explain how these susceptibilities can be approximated as sums of *per-token susceptibilities*. This provides a useful tool (see Figure 1) for exploring the internal structure of a model, as revealed by susceptibilities, by studying text samples such as the one shown in Figure 1.

Susceptibilities build on a series of papers establishing singular learning theory and local learning coefficient estimation as principled tools for understanding neural networks and their development (Hoogland et al., 2025; Wang et al., 2024; Urdshals and Urdshals, 2025; Carroll et al., 2025). Ultimately we view these techniques as leading to scalable and theoretically principled tools for interpretability in large neural networks, parallel to existing approaches within mechanistic interpretability such as ablations or sparse auto-encoders.

However in this paper our goals are modest. We define susceptibilities and perform some basic sanity checks on the technique in a small language model that we understand well from prior work (Hoogland et al., 2025; Wang et al., 2024). This allows us to calibrate the results from susceptibilities with other techniques, such as ablations, that are better understood.

We make the following observations:

- **Different parts of the model respond differently.** The premise of susceptibilities is that if we have a diverse enough set of perturbations of the data distribution, we can elicit internal structure. The first hurdle the technique must clear, therefore, is that a natural class of perturbations of the data distribution elicits differentiated responses from the attention heads in our model. We find that this to be the case (Section 4.1).
- **Susceptibilities are not redundant.** Next we check that susceptibilities are not highly correlated with losses or losses after ablation (Section 4.3). Although this is not an exhaustive comparison with other interpretability techniques, it does suggest that susceptibilities may be accessing information about models that is not exposed by other common interpretability techniques.
- **Per-token susceptibilities are useful.** We can view the susceptibility as “made up” of susceptibilities associated to particular tokens in context, and since these can be visualized this yields immediate interpretability benefits (see Figure 1). We demonstrate this technique

in a simple example, where we explain why a particular attention head is an outlier using per-token susceptibilities (Section 4.5).

- **Positive vs negative.** As we might expect from the analogy with magnetic susceptibility, susceptibilities can be both positive and negative. Anecdotally we see a difference between the kind of tokens that have negative vs positive susceptibility. To illustrate this more clearly, we provide in Section 4.6 some examples of single tokens that have semantically distinct negative and positive per-token susceptibilities.
- **Structural inference passes a basic test.** Eventually we hope to follow the paradigm in condensed matter physics of using susceptibilities to infer facts about internal structure in neural networks. In this paper we run a minimal test of the ideas and obtain preliminary but encouraging results (Section 4.2).

In outline, the paper begins with a presentation of the theory of susceptibilities (Section 2), then presents our methodology for realizing the technique scalably for language models (Section 3) before presenting the results (Section 4) which are followed by the related work, discussion and conclusion.

## 2 Theory

We adopt the notation and approach of Watanabe (2007), Watanabe (2018). In a typical Bayesian statistical model, we consider the model-truth-prior triplet

$$(p(x, y|w), q(x, y), \varphi(w)), \quad (3)$$

where  $q(x, y) = q(y|x)q(x)$  is the true data-generating mechanism,  $p(x, y|w) = p(y|x, w)q(x)$  is the posited model with parameter  $w \in W \subset \mathbb{R}^d$  representing the neural network weights, and  $\varphi$  is a prior on  $w$ . We assume that  $q(x, y) > 0$  and  $p(y|x, w) > 0$  for all  $(x, y) \in X \times Y$  and  $w \in W$ . Let the sample spaces  $X, Y$  be measure spaces (e.g. sequences of tokens with the counting measure) so that  $q(x, y)$  is a probability density with respect to the measure  $\mu$  on  $X \times Y$ .

Given a training dataset of  $n$  input-output pairs,  $D_n = \{(x_i, y_i)\}_{i=1}^n$ , drawn i.i.d. from  $q(x, y)$ , we define the sample negative log-likelihood function as

$$L_n(w) = -\frac{1}{n} \sum_{i=1}^n \log p(y_i|x_i, w), \quad (4)$$

and its theoretical counterpart, the average negative log-likelihood or *population loss*, as

$$L(w) = -\mathbb{E}_{q(x,y)} \log p(y|x, w). \quad (5)$$

The *Bayesian posterior* at inverse temperature  $\beta$  is given by

$$p^\beta(w|D_n) = \frac{1}{Z_n^\beta} \exp\{-n\beta L_n(w)\} \varphi(w), \quad \text{where} \quad Z_n^\beta = \int \exp\{-n\beta L_n(w)\} \varphi(w) dw. \quad (6)$$

When  $\beta = 1$  we drop the superscripts and write  $p(w|D_n), Z_n$ . The *quenched posterior* at inverse temperature  $\beta > 0$  is

$$p_n^\beta(w) = \frac{1}{Z_n^\beta} \exp\{-n\beta L(w)\} \varphi(w) \quad \text{where} \quad Z_n^\beta = \int \exp\{-n\beta L(w)\} \varphi(w) dw. \quad (7)$$

In this paper we work with the quenched posterior since this means that derivatives of expectation values with respect to  $h$  are mathematically easier to deal with. We leave a complete treatment for later work. Unless specified otherwise, covariances and expectation values in this paper are defined with respect to quenched posteriors. We can absorb  $n\beta$  into a single inverse temperature, but since  $n$  is an integer it is convenient to keep this component explicitly.

### 2.1 Variation in the truth

We consider a one-parameter variation of the true distribution of the following form. Let  $H \subseteq \mathbb{R}$  be some open interval containing 0 and for  $h \in H$  let  $q_h(x, y)$  be a probability density with respect to

the measure  $\mu$  on  $X \times Y$ . We assume that  $h \mapsto q_h$  is differentiable as a map from  $H$  to  $L^1(X \times Y, \mu)$ . That is there is  $g_h(x, y) \in L^1(X \times Y, \mu)$  such that for all  $h \in H$

$$\lim_{\delta \rightarrow 0} \int_{X \times Y} \left| \frac{q_{h+\delta}(x, y) - q_h(x, y)}{\delta} - g_h(x, y) \right| d\mu(x, y) = 0. \quad (8)$$

We write  $\frac{\partial}{\partial h} q_h$  for  $g_h$ . One-sided derivatives are defined in the obvious way. In the rest of the paper we write  $dx dy$  for  $d\mu(x, y)$ .

Given a training dataset of  $n$  input-output pairs,  $D_n^h = \{(x_i, y_i)\}_{i=1}^n$ , drawn i.i.d. from  $q_h(x, y)$ , we define  $L_n^h(w)$  to be as in (4) noting that this is a random function that depends on  $q_h$  only through  $D_n^h$ . The average negative log-likelihood is

$$L^h(w) = -\mathbb{E}_{q_h(x, y)} \log p(y|x, w).$$

The quenched posterior for  $q_h$  is

$$p_n^\beta(w|h) = \frac{1}{Z_n^{\beta, h}} \exp\{-n\beta L^h(w)\} \varphi(w) \quad \text{where} \quad Z_n^{\beta, h} = \int \exp\{-n\beta L^h(w)\} \varphi(w) dw. \quad (9)$$

The most common kind of one-parameter variation in the true distribution is a mixture. Let  $q'$  be another probability density on  $X \times Y$ . For instance, if  $q$  is the hypothetical distribution represented by the Pile, let  $q'$  denote a ‘‘code heavy’’ variant. Given  $h \in [0, 1]$  we define

$$q_h = (1 - h)q + hq'. \quad (10)$$

Note that the parameter  $h$  comes with a fixed scale, since it indexes a mixture. Then the (one-sided) derivative in (8) exists and is the function

$$(x, y) \in X \times Y \mapsto g_h(x, y) = q'(x, y) - q(x, y). \quad (11)$$

## 2.2 Susceptibilities

A *response function* measures how some observable changes under a small external perturbation or variation of a controlling parameter. In our Bayesian setting, suppose we pick an observable (a function on parameter space)  $\phi(w)$ . We then consider its (quenched) posterior expectation, where we denote by  $h$  some hyperparameter

$$\langle \phi \rangle_{\beta, h} = \int \phi(w) p_n^\beta(w|h) dw. \quad (12)$$

We also allow the observable  $\phi$  to vary with  $h$ . If we drop  $h$  from the notation it means we are computing expectations with respect to the *unperturbed* (quenched) posterior (i.e.  $h = 0$ )

$$\langle \phi \rangle_\beta = \int \phi(w) p_n^\beta(w) dw. \quad (13)$$

A small change in the hyperparameter  $h$  induces a shift in the posterior as a distribution, and some aspect of this shift is captured by the shift in the expectation value  $\langle \phi \rangle_{\beta, h}$  across all suitable observables  $\phi$ . The linear response is:

**Definition 2.1.** The *susceptibility* of  $\phi$  to the perturbation  $q_h$  at inverse temperature  $\beta$  is

$$\chi = \frac{1}{n\beta} \frac{\partial}{\partial h} \langle \phi \rangle_{\beta, h} \Big|_{h=0}. \quad (14)$$

Note that this is a function of  $n$  and we view  $\beta$  as fixed.

*Remark 2.2.* Since the scale of the parameter  $h$  is arbitrary, there is a sense in which susceptibilities are only well-defined up to a rescaling. This is easy to understand if we consider multiple variations of the form (10), say  $q \rightarrow q'$  and  $q \rightarrow q''$  where the KL divergence between  $q, q''$  is much larger than between  $q, q'$ . By default therefore we should not read too much into comparisons of *magnitudes* of susceptibilities across different variations of the true distribution.

For example if we set  $\bar{h} = \frac{h}{\kappa}$  for some  $\kappa > 0$  then

$$\frac{1}{n\beta} \frac{\partial}{\partial \bar{h}} \langle \phi \rangle_{\beta, \bar{h}} \Big|_{\bar{h}=0} = \frac{\kappa}{n\beta} \frac{\partial}{\partial h} \langle \phi \rangle_{\beta, h} \Big|_{h=0} = \kappa \chi. \quad (15)$$

**Lemma 2.3.** *The susceptibility for an observable  $\phi_h$  is computed by*

$$\chi = -\text{Cov}_\beta [\phi, \Delta L] + O\left(\frac{1}{n}\right) \quad (16)$$

where  $\phi = \phi_0$  and

$$\text{Cov}_\beta [\phi, \Delta L] = \langle \phi \Delta L \rangle_\beta - \langle \phi \rangle_\beta \langle \Delta L \rangle_\beta, \quad \Delta L = \left. \frac{\partial L^h}{\partial h} \right|_{h=0}. \quad (17)$$

*Proof.* Let  $Z_n^{\beta, h}$  be as in Section 2.1. Then

$$n\beta \chi = \left. \frac{\partial}{\partial h} \langle \phi_h \rangle_{\beta, h} \right|_{h=0} \quad (18)$$

$$= \left. \frac{\partial}{\partial h} \left[ \frac{1}{Z_n^{\beta, h}} \int \phi_h(w) \exp(-n\beta L^h(w)) \varphi(w) dw \right] \right|_{h=0} \quad (19)$$

$$= \left. \frac{\partial}{\partial h} \frac{1}{Z_n^{\beta, h}} \right|_{h=0} Z_n^\beta \langle \phi \rangle_\beta + \left\langle \left. \frac{\partial \phi_h}{\partial h} \right|_{h=0} \right\rangle_\beta - n\beta \langle \phi \Delta L \rangle_\beta. \quad (20)$$

Since

$$\left. \frac{\partial}{\partial h} \frac{1}{Z_n^{\beta, h}} \right|_{h=0} = -\frac{1}{(Z_n^{\beta, h})^2} \int \left[ -n\beta \frac{\partial}{\partial h} L^h(w) \right] \exp(-n\beta L^h(w)) \varphi(w) dw \quad (21)$$

we have

$$\left. \frac{\partial}{\partial h} \frac{1}{Z_n^{\beta, h}} \right|_{h=0} = \frac{n\beta}{Z_n^\beta} \langle \Delta L \rangle_\beta. \quad (22)$$

Combining (20) and (22) we obtain

$$n\beta \chi = n\beta \langle \phi \rangle_\beta \langle \Delta L \rangle_\beta - n\beta \langle \phi \Delta L \rangle_\beta + \left\langle \left. \frac{\partial \phi}{\partial h} \right|_{h=0} \right\rangle_\beta.$$

Dividing through by  $n\beta$  gives the result.  $\square$

Note that even though the observable  $\phi$  varies with  $h$ , this variation only contributes as a lower order term to the susceptibility. Further, from the lemma we learn that the susceptibility can be estimated in practice *using only samples from the unperturbed posterior*. That is, using the same kind of samples that we generate anyway in the course of producing LLC estimates.

Next we define the primary class of observables to be considered in this paper. We consider statistical models  $p(y|x, w)$  parametrized by neural networks with weights  $w \in W$ . Then by a *subnetwork* we mean a subset  $C$  of these weights (e.g. an attention head in a transformer). More formally, a subnetwork is a product decomposition  $W = U \times C$  with  $U$  the parameters not in the subnetwork.

**Definition 2.4.** Given a subnetwork  $C$  with  $W = U \times C$  and a chosen parameter  $w^* = (u^*, v^*)$  write  $w = (u, v)$  for a general coordinate and define

$$\phi_C(w) := \delta(u - u^*) \left[ L(w) - L(w^*) \right]. \quad (23)$$

This observable vanishes if the parameter  $w$  varies from  $w^*$  in any of the directions not involved in the subnetwork, and otherwise measures the effect on the empirical loss of variations in the subnetwork.

**Lemma 2.5.** *With  $q_h$  the variation in (10) we have*

$$\Delta L(w) = L^1(w) - L(w) \quad (24)$$

where  $L^1(w)$  and  $L(w)$  are  $L^h(w)$  with  $h = 0$  and  $h = 1$ , respectively.

*Proof.* We compute

$$\begin{aligned} \Delta L &= \left. \frac{\partial}{\partial h} L^h \right|_{h=0} \\ &= -\frac{\partial}{\partial h} \int q_h(x, y) \log p(y|x, w) dx dy \\ &= -\int \frac{\partial}{\partial h} q_h(x, y) \log p(y|x, w) dx dy \\ &= -\int (q'(x, y) - q(x, y)) \log p(y|x, w) dx dy \\ &= L^1(w) - L(w) \end{aligned}$$

using (11). □

Hence in the case where the variation in  $q$  is as in (10) and the observable is  $\phi = \phi_C$ , we have

$$\chi = -\text{Cov}_\beta \left[ \delta(u - u^*) \{L(w) - L(w^*)\}, L^1(w) - L(w) \right] + O\left(\frac{1}{n}\right). \quad (25)$$

This is the covariance of two differences of population losses: one measures how much a variation in  $w$  within the subnetwork increases the loss on the original data distribution  $q$  relative to the loss at  $w^*$ , and the other measures how much a variation in  $w$  changes the *gap* between the loss on  $q$  and  $q'$ .

*Remark 2.6.* The Bayesian susceptibility introduced above is the direct analogue of susceptibilities in physics, such as the magnetic susceptibility. We recall briefly the linear response of a spin system placed in an external magnetic field  $H$ . With energy  $E(\sigma)$  and magnetisation  $M(\sigma) = \sum_i \sigma_i$ , the field-perturbed Boltzmann weight is

$$p_H(\sigma) = \frac{1}{Z_H} \exp[-\beta(E(\sigma) - H M(\sigma))], \quad Z_H = \int \exp[-\beta(E - H M)] d\sigma.$$

The *magnetic susceptibility* is the first derivative of the equilibrium magnetisation,

$$\chi_{\text{mag}} = \frac{\partial}{\partial H} \langle M \rangle_H \Big|_{H=0}, \quad \langle M \rangle_H = \int M(\sigma) p_H(\sigma) d\sigma.$$

Its sign carries immediate physical meaning:

Sign of $\chi_{\text{mag}}$	Interpretation
$\chi_{\text{mag}} > 0$	(paramagnetism) spins align with $H$ ; response <i>reinforces</i> the field
$\chi_{\text{mag}} = 0$	(insensitive) system insensitive or already saturated
$\chi_{\text{mag}} < 0$	(diamagnetism) induced currents oppose $H$ ; response <i>cancel</i> s the field

The Bayesian susceptibility  $\chi$  parallels the magnetic susceptibility, with the probe parameter  $h$  replacing the magnetic field strength  $H$  and  $\phi(w)$  replacing the magnetization  $M(\sigma)$ .

It is somewhat subtle to interpret the sign of susceptibilities; here we briefly summarize Section 2.4 in the case that increasing  $h$  (moving from  $q$  to  $q'$ ) *decreases* the frequency of some pattern  $\alpha$  (for example some common  $n$ -grams in general Internet text are less frequent in code or formal legal documents). Using  $\chi = -\text{Cov}_\beta[\phi, \Delta L]$  we can give the following interpretation:

Sign of $\chi$	Interpretation for a subnetwork $C$
$\chi > 0$	(“paramagnetic”) $C$ is <i>attracted</i> : variations in $C$ that hurt the baseline loss tend to hurt prediction of the pattern $\alpha$ .
$\chi = 0$	(insensitive) Loss changes in $C$ are uncorrelated with the probe.
$\chi < 0$	(“diamagnetic”) $C$ is <i>repelled</i> : variations in $C$ that improve the baseline loss tend to hurt prediction of the pattern $\alpha$ .

Note that, unlike bulk matter,  $\chi$  can vary in sign *within a single model*: different internal structures may respond in opposite ways to the same data perturbation, revealing functional heterogeneity. For a good concise introductions to linear response theory see [Altland and Simons \(2010\)](#).

### 2.3 Local Susceptibility

The major practical obstacle to computing susceptibilities for large-scale neural networks is the *difficulty of sampling* from the posterior  $p^\beta(w|D_n)$ . This challenge is akin to that faced in estimating the local learning coefficient (LLC): naive MCMC approaches (e.g. full-batch Metropolis-Hastings) are prohibitively expensive. However, the work of [Lau et al. \(2024\)](#) and subsequent papers suggests that *localizing* the posterior around a point of interest makes Stochastic Gradient Langevin Dynamics (SGLD) sampling sufficiently efficient and accurate for many practical purposes.

Let  $w^*$  be a local minima of  $L(w)$ . Recall that the estimated LLC is defined by

$$\hat{\lambda}(w^*) = n\beta \left[ \mathbb{E}_{w|w^*, \gamma}^\beta [L_n(w)] - L_n(w^*) \right], \quad (26)$$

where  $\mathbb{E}_{w|w^*,\gamma}^\beta$  is the expectation with respect to the Gibbs posterior (Bissiri et al., 2016)

$$p(w; w^*, \beta, \gamma) \propto \exp \left\{ -n\beta L_n(w) - \frac{\gamma}{2} \|w - w^*\|_2^2 \right\}. \quad (27)$$

where  $w^*$  is a (local) minimizer of  $L$ ,  $\gamma > 0$  enforces that sampling remains in a small neighborhood of  $w^*$  and  $\beta > 0$  is the inverse temperature. We also define a quenched version of this distribution

$$p(w; w^*, \beta, \gamma, h) \propto \exp \left\{ -n\beta L^h(w) - \frac{\gamma}{2} \|w - w^*\|_2^2 \right\}. \quad (28)$$

The *local (quenched) expectation value* of  $\phi$  at  $w^*$  and at inverse temperature  $\beta$  is

$$\langle \phi; w^* \rangle_{\beta, h} := \int \phi(w) p(w; w^*, \beta, \gamma, h) dw.$$

**Definition 2.7.** We define the *local susceptibility* at inverse temperature  $\beta$  to be

$$\chi(w^*) = \frac{1}{n\beta} \left. \frac{\partial}{\partial h} \langle \phi; w^* \rangle_{\beta, h} \right|_{h=0}. \quad (29)$$

*Remark 2.8.* Given a target distribution  $q'(x, y)$  and the mixture (10) we obtain  $\Delta L = L^1(w) - L(w)$  from Lemma 2.5. However, if the difference between  $q'$  and  $q$  is large,  $w^*$  may not be a local minima of  $L^1(w)$ . The likelihood of this being a reasonable assumption increases as we move  $q'$  closer to  $q$ .

Since susceptibilities are in any case infinitesimal, this suggests that we replace the original variation from  $q$  to  $q'$  with a variation from  $q$  to  $(1 - \delta h)q + \delta h q'$  for some small  $\delta h$ . In this case the mixture is

$$\begin{aligned} h \in [0, 1] &\mapsto (1 - h)q + h(1 - \delta h)q + h\delta h q' \\ &= (1 - h\delta h)q + h\delta h q'. \end{aligned}$$

In this case, again by Lemma 2.5, we will have that  $\Delta L$  is a finite difference

$$\Delta L(w) := L^{\delta h}(w) - L(w).$$

For local susceptibilities we always choose a variation which is sufficiently small, in this sense.

*Remark 2.9.* Suppose we approximate the derivative in the local susceptibility by a difference quotient for some small  $\delta h \in (0, 1)$

$$\chi_{\text{finite}}(w^*) := \frac{1}{n\beta} \frac{1}{\delta h} \left[ \langle \phi; w^* \rangle_{\beta, \delta h} - \langle \phi; w^* \rangle_{\beta} \right].$$

When the observable  $\phi$  is associated to a subnetwork  $C$  as in Theorem 2.4 then the expectations in question are, up to scalars, estimates of the weight- and data-refined LLCs as introduced in Wang et al. (2024) once we replace the quenched posteriors by the ordinary ones, since

$$\mathbb{E}_{w|w^*,\gamma}^\beta \left[ \delta(u - u^*) \{ L_n^h(w) - L_n^h(w^*) \} \right] = \frac{1}{n\beta} \hat{\lambda}(w^*; q_h, C).$$

Hence  $\chi_{\text{finite}}(w^*)$  is related to the difference quotient

$$\frac{1}{(n\beta)^2} \frac{1}{\delta h} \left[ \hat{\lambda}(w^*; q_{\delta h}, C) - \hat{\lambda}(w^*; q, C) \right]$$

which measures a rate of change of the refined LLC as a function of the shift in the data distribution.

## 2.4 Modes and Probes

In the introduction we sketched out a standard paradigm in many parts of physics: subject a system to various kinds of perturbations, measure the responses, and make inferences on the basis of this data. In Section 2.2 we introduced the local susceptibility for a variation in the data distribution and a subnetwork in the model. However, it is not currently clear from what we have said so far how to use this to infer information about internal structure in the model. In this section we explain, in the setting of a sequence model, how to do this.

We adopt the setting of (Chen and Murfet, 2025). That paper explains how to think about the true distribution over sequences as a tensor, and use tensor decomposition methods to produce natural orthonormal bases of function space. We fix an alphabet of symbols  $\Sigma$  and let

$$\mathcal{H} = \mathcal{H}_{k,l} = L^2(\Sigma^k, q_k; \mathbb{R}^{\Sigma^l})$$

be the function space. We set  $X = \Sigma^k, Y = \Sigma^l$  with the counting measure,  $q(x, y)$  is the true distribution for  $x \in \Sigma^k, y \in \Sigma^l$  and  $q(x) = q_k(x)$  denotes the true distribution over sequences of length  $k$ . Let  $\mathcal{C} \in \mathcal{H}$  be the function corresponding to the true conditional probabilities

$$\mathcal{C}(x) = \sum_{y \in \Sigma^l} q(y|x)y, \quad \forall x \in \Sigma^k. \quad (30)$$

As explained in Chen and Murfet (2025) by applying tensor decomposition methods such as SVD to  $\mathcal{C}$  we obtain a natural orthonormal basis  $\{e_{\alpha\beta}\}_{\alpha \in \Lambda, \beta \in \Lambda^{++}}$  of  $\mathcal{H}$ . Here  $\Lambda$  indexes right singular vectors,  $\Lambda^+$  indexes left singular vectors for nonzero singular values, and  $\Lambda^{++} \supseteq \Lambda^+$  is an extended set of indices associated to an arbitrary extension of the left singular vectors to an orthonormal basis of  $\mathbb{R}^{\Sigma^l}$ .<sup>\*</sup> The examples given in Chen and Murfet (2025) justify identifying such modes with *atomic patterns* in the data distribution.

Let us consider a variation of the true distribution  $q(x, y)$  which is a ‘‘concept shift’’, that is, we vary the conditional distribution  $q(y|x)$  but not  $q(x)$ . Let us write  $q'(y|x)$  for some other conditional distribution and set  $q'(x, y) = q'(y|x)q(x)$ . Let  $\mathcal{C}'$  denote the equivalent of (30) but for  $q'$ .

**Definition 2.10.** We say a variation in the true distribution of the form

$$\mathcal{C}' - \mathcal{C} = \sum_{\alpha \in \Lambda} c^\alpha e_{\alpha\alpha} \quad (31)$$

for some  $c^\alpha \in \mathbb{R}$  is *mode aligned*.

**Definition 2.11.** Given  $w \in W$  we define  $\Phi(w) \in \mathcal{H}$  by

$$\Phi(w)(x) = - \sum_{y \in \Sigma^l} \log p(y|x, w) y.$$

Given  $\alpha \in \Lambda$  we define  $\Phi_\alpha : W \rightarrow \mathbb{R}$  by

$$\Phi_\alpha(w) = \langle \Phi(w), e_{\alpha\alpha} \rangle_{\mathcal{H}}.$$

**Lemma 2.12.** For a mode aligned concept shift as above

$$\chi = - \sum_{\alpha \in \Lambda} c^\alpha \text{Cov}_\beta [\phi, \Phi_\alpha] + O\left(\frac{1}{n}\right).$$

*Proof.* We compute that

$$\begin{aligned} \Delta L &= - \int (q'(y|x) - q(y|x))q(x) \log p(y|x, w) dx dy \\ &= - \sum_{\alpha \in \Lambda} c^\alpha \int e_{\alpha\alpha}(x)(y)q(x) \log p(y|x, w) dx dy \\ &= \sum_{\alpha \in \Lambda} c^\alpha \langle \Phi(w), e_{\alpha\alpha} \rangle_{\mathcal{H}} \end{aligned}$$

so the conclusion follows from Lemma 2.3 and bilinearity of the covariance.  $\square$

Therefore in this setting the fundamental quantities are the covariances of  $\phi$  with  $\Phi_\alpha$ . Note that if  $\mathcal{C}' - \mathcal{C} \propto e_{\alpha\alpha}$ , that is, the deformation of the true distribution is *pure* in the sense it affects only a single mode, then  $\Delta L \propto \Phi_{\alpha\alpha}$ . Note however that generally adding a multiple of  $e_{\alpha\alpha}$  to  $\mathcal{C}$  produces a valid function in  $\mathcal{H}$  but not a valid conditional distribution; thus the  $\Phi_\alpha$  are  $\Delta L$  for ‘‘imaginary’’ deformations of the true distribution. We call the resulting covariances *pure susceptibilities*:

<sup>\*</sup>For consistency with Chen and Murfet (2025) we continue to use  $\beta$  as an index, note this is distinct from the inverse temperature.

**Definition 2.13.** For any  $\alpha \in \Lambda$  we call

$$\chi_\alpha^{\text{pure}} = -\text{Cov}_\beta [\phi, \Phi_\alpha]$$

the *pure susceptibility* of  $\phi$  at inverse temperature  $\beta$  to the mode  $\alpha$ . Note that this depends on the observable  $\phi$  but not on the variation in the data distribution.

From Lemma 2.12 we obtain that the susceptibility for any concept shift is of the form

$$\chi = \sum_{\alpha \in \Lambda} c^\alpha \chi_\alpha^{\text{pure}} \quad (32)$$

for some coefficients  $c^\alpha$ .

**Absolute bigrams.** If  $\sigma \in \Sigma^k, \tau \in \Sigma^l$  form an *absolute bigram*  $\sigma\tau$  for  $q$  in the sense of [Chen and Murfet \(2025\)](#) then this corresponds to a mode  $\alpha$  with singular value  $s_\alpha = q(\sigma)^{1/2} = q(\sigma\tau)^{1/2}$ . Suppose  $\sigma\tau$  is an absolute bigram also for  $q'$ , then  $c^\alpha = q'(\sigma\tau)^{1/2} - q(\sigma\tau)^{1/2}$  and

$$\Phi_\alpha(w) = \langle \Phi(w), e_{\alpha\alpha} \rangle_{\mathcal{H}} = -\log p(\tau|\sigma, w)q(\sigma)^{1/2}. \quad (33)$$

Note that  $-\log p(\tau|\sigma, w)$  is the cross-entropy loss of the model on predicting the bigram. Hence the contribution of any absolute bigram to  $\Delta L$  is

$$c^\alpha \Phi_\alpha(w) = \log p(\tau|\sigma, w)q(\sigma) \left(1 - \sqrt{\frac{q'(\sigma\tau)}{q(\sigma\tau)}}\right).$$

Let us now consider the meaning of the pure susceptibility for the observable  $\phi_C$  of Theorem 2.4 with respect to the absolute bigram mode  $\alpha$ . We have

$$\chi_\alpha^{\text{pure}} = -\text{Cov}_\beta \left[ \delta(u - u^*) [L(w) - L(w^*)], \Phi_\alpha \right].$$

Let us consider a variation in  $w = (u, v)$  that only varies  $v$ . Such a variation increases  $\Phi_\alpha$  if and only if it makes the model worse at predicting  $\tau$  given  $\sigma$ , that is, if it makes the model worse at predicting the bigram. Such a variation increases  $L - L(w^*)$  if and only if it makes the overall loss of the network higher, that is, it makes the model worse at prediction in general. In the following we write *pattern for bigram* so that the general philosophy is clearer.

**Positive covariance.** These two functions of  $w$  (meaning  $\Phi_\alpha$  and  $L - L(w^*)$ ) have large positive covariance if *variations in  $C$  tend to make the model worse at prediction if and only if they make the model worse at predicting this particular pattern*. This seems plausibly true if the main role of the subnetwork  $C$  is predicting the pattern (it does not preclude that other components are also involved). In this case  $\chi_\alpha^{\text{pure}}$  is large and *negative*. Suppose now that the variation  $q \rightarrow q'$  increases the probability of the pattern. Then  $c^\alpha > 0$  so  $c^\alpha \chi_\alpha^{\text{pure}} < 0$  and this pattern contributes *negatively* to the overall susceptibility. The sign is reversed if the pattern is less frequent in  $q'$  than in  $q$ .

**Negative covariance.** In the other direction, these two functions have large negative covariance if *variations in  $C$  tend to make the model better at prediction if and only if they make the model worse at predicting this particular pattern*. That is,  $C$  is a *counter-weight* to the pattern  $\alpha$ . For example,  $C$  might be optimizing for something that conflicts with predicting the pattern (e.g. a syntactic rule may conflict with a bigram). In this case  $\chi_\alpha^{\text{pure}}$  is large and *positive*. If further the variation  $q \rightarrow q'$  increases the probability of the pattern then  $c^\alpha \chi_\alpha^{\text{pure}} > 0$  so this pattern contributes *positively* to the overall susceptibility. The sign is reversed if the pattern is less frequent in  $q'$  than in  $q$ .

**Zero covariance.** These two functions of  $w$  have zero covariance if *variations in  $C$  which tend to make the model worse at prediction are equally likely to make the model better or worse at predicting this particular pattern*. That is, whatever contributions  $C$  makes to prediction seem independent of predicting the pattern. In this case  $\chi_\alpha^{\text{pure}} = 0$ .

In general it is difficult to classify by hand the modes of  $q$  beyond simple examples like absolute bigrams, although see [Chen and Murfet \(2025\)](#) for some empirical examples. Moreover, the variations  $q \rightarrow q'$  that we consider in this paper, with  $q$  the Pile and  $q'$  a Pile subset, are unlikely to be concept shifts and we do not expect that all patterns in the data distribution are necessarily captured by modes in the above sense. Nonetheless, the decomposition in (32) and the characterization above of positive, negative and zero covariance provide some useful intuition about susceptibilities.

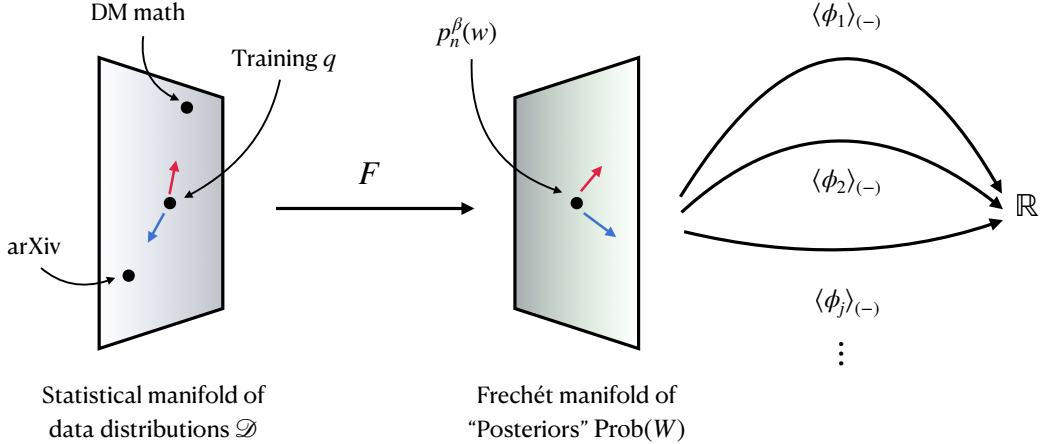


Figure 2: **Susceptibilities as components of a tangent map.** We can think of susceptibilities as components of the tangent map from data distributions to the expectations of a family of observables with respect to the posterior formed for that data distribution, with a fixed model. In this diagram we indicate  $q \in \mathcal{D}$ , the training distribution, and tangent vectors in this space corresponding to the mixtures with `arxiv` and `dm_mathematics`. The tangent map of  $F$  sends these tangent vectors to tangent vectors in the space of “posteriors”.

## 2.5 Structural Inference

We explain how, in the setting of Section 2.4, we can use a set of variations in the data distribution to infer something about the modes. Under the hypothesis that internal structures in models are associated with modes (or coarse-grained sets of modes, like predicting a bracket `} , ) , )` in some set of contexts) this allows us to infer something about internal computational structure. We refer to this as *structural inference*.

Let  $\{C_j\}_{j \in \mathcal{H}}$  be a finite set of subnetworks with associated observables  $\phi_j$  (e.g. attention heads) and  $\{q_d\}_{d \in \mathcal{D}}$  a finite set of data distributions with associated variations from  $q$  by taking mixtures (e.g. Pile subsets like `github`). We refer to this as a *probe set* and the individual data distributions as *probe distributions*. We think of  $q_d$  as being accessible variations in the data distribution, which vary the distribution of many modes.

In Section 2.4 the notation does not reflect the choice of observable. We denote by  $\chi_j^d$  the susceptibility for  $q_d$  and observable  $\phi_j$ . We denote by  $\chi_{\alpha,j}^{\text{pure}}$  the pure susceptibility for a mode  $\alpha$  and the observable  $\phi_j$ . Ideally we would like to measure  $\chi_{\alpha,j}^{\text{pure}}$  but in practice we do not have the ability to sample from variations of the data distribution which only affect single modes. However, by Lemma 2.12

$$\chi_j^d = \sum_{\alpha \in \Lambda} c^{d,\alpha} \chi_{\alpha,j}^{\text{pure}} \quad (34)$$

where we note that  $c^{d,\alpha}$  is from Definition 2.10 and does not depend on  $j$ . This is a matrix equation

$$X = CP \quad (35)$$

where  $X$  is the  $|\mathcal{D}| \times |\mathcal{H}|$  matrix with entries  $\chi_j^d$ ,  $C$  is the  $|\mathcal{D}| \times |\Lambda|$  matrix with entries  $c^{d,\alpha}$  and  $P$  is the  $|\Lambda| \times |\mathcal{H}|$  matrix with entries  $\chi_{\alpha,j}^{\text{pure}}$ . We refer to  $X$  as the *data matrix* or *response matrix*. Then  $C$  gives the coefficients of each variation of the data distribution in each mode (e.g. for an absolute bigram  $\sigma\tau$  as above the entry in position  $d, \alpha$  gives the difference in square-root probability of the bigram in the variation  $d$ ) and  $P$  is the matrix of pure susceptibilities. More informally, we think of  $C$  as the *coupling coefficients* between variations in the data and modes, and  $P$  as the coupling coefficients between observables and modes.

The quantities  $\chi_j^d$  may be estimated from data, as we will explain in Section 3.1. That is, we may assume an empirical estimate of the data matrix  $X$ . On the other hand  $C, P$  are not directly observable because it is intractable to determine the complete set of modes of a complex distribution. However

(35) suggests a way to apply methods of data analysis to the matrix  $X$  in order to *infer* the modes and their couplings to the observables.

To summarize the conceptual framework: we imagine the Bayesian posterior as statistical mechanical system which we subject to a range of small “external fields” and then measure the results using a range of observables. The  $q_d$  are the external fields (probes) and the  $\phi_j$  are the observables. The idea, borrowed from physics, is that *internal structure is by definition the patterns that manifest in the responses of a system to external perturbations, as measured by natural observables* (Altland and Simons, 2010, §7). The responses are by definition the entries of the matrix  $X$ , and so to a first approximation, internal structure in the network means the linear algebraic structure of  $X$ .

This is all summarized neatly by Figure 2. We can define a smooth map  $F$  which sends a distribution  $q' \in \mathcal{D}$  over sequences of tokens to (for fixed  $n, \beta$ ) the quenched and tempered posterior distribution  $F(q') = p_n^\beta(w|q')$  as a point in the Frechét manifold  $\text{Prob}(W)$  of positive densities of integral 1 on  $W$  (Bauer et al., 2016). Suitably well-behaved observables  $\phi_j : W \rightarrow \mathbb{R}$  define, by taking expectations, functions on this manifold. Given a set  $\{\phi_j\}_{j \in \mathcal{H}}$  we therefore obtain a map

$$G = \begin{pmatrix} \langle \phi_1 \rangle_{(-)} \\ \vdots \\ \langle \phi_j \rangle_{(-)} \\ \vdots \end{pmatrix} : \text{Prob}(W) \rightarrow \mathbb{R}^{\mathcal{H}}.$$

Composing with  $F$  gives a map  $\mathcal{D} \rightarrow \mathbb{R}^{\mathcal{H}}$  whose tangent map at  $q$  is

$$T_q(G \circ F) = T_{p_n^\beta(w)}(G) \circ T_q(F) : T_q \mathcal{D} \rightarrow T_{\langle \phi \rangle} \mathbb{R}^{\mathcal{H}} \quad (36)$$

where  $\langle \phi \rangle$  denotes the vector of expectation values of all observables with respect to the unperturbed (quenched, tempered) posterior  $p_n^\beta(w)$ . By definition this linear map, or rather its restriction to the subspace of the tangent space spanned by the tangents to the mixtures with the  $q_d$ , has as its matrix the (transposed) response matrix  $X^T$  (up to a factor of  $n\beta$ ). The relationship between the matrix factorizations in (35) and (36).

### 3 Methodology

#### 3.1 Estimating the Local Susceptibility

By Lemma 2.3 we can write

$$\chi(w^*) = -\langle \phi \Delta L; w^* \rangle_\beta + \langle \phi; w^* \rangle_\beta \langle \Delta L; w^* \rangle_\beta + O\left(\frac{1}{n}\right). \quad (37)$$

We fix a mixture percentage  $\delta h \in (0, 1)$  and, as in Remark 2.8, approximate  $\Delta L$  by

$$\Delta L_n(w) := L_n^{\delta h}(w) - L_n(w) \quad (38)$$

for some dataset size  $n$ . We also replace the expectations in (37) with respect to the quenched posterior (28) with expectations with respect to the ordinary localized posterior (27) involving  $L_n$ .

*Remark 3.1.* It would also be natural to include a factor  $1/\delta h$  here so that  $\Delta L_n(w)$  is a finite difference quotient. This could be motivated by the principle given in Remark 2.2 that we should rescale the deformation parameter  $h$  since our interval is “really” of length  $\delta h$ .

We compute  $L_n(w) = L_n^0(w)$  by drawing a sample from the original data distribution  $q$ , and  $L_n^{\delta h}(w)$  by drawing a set of samples of size  $n$ , consisting of a mixture of samples from the unperturbed data distribution and samples from the perturbed data distribution (the mixture being controlled by  $\delta h$ ). Given approximate samples  $\{w_t\}_{t=1}^r$  from the (unperturbed and unquenched) localized posterior with parameter  $\beta$  we compute our estimate of the susceptibility to be

$$\hat{\chi}(w^*) := -\frac{1}{r} \sum_{t=1}^r \left[ \phi(w_t) \Delta L_n(w_t) \right] + \frac{1}{r^2} \left[ \sum_{t=1}^r \phi(w_t) \right] \left[ \sum_{t=1}^r \Delta L_n(w_t) \right]. \quad (39)$$

Typically we further average this quantity over multiple chains  $\{w_t\}_{t=1}^r$ . To be clear, these are the *same kind of samples* we would use to compute an estimate of the LLC at inverse temperature  $\beta$  for

the model  $w^*$  with respect to the unperturbed data distribution as in [Lau et al. \(2024\)](#), [Wang et al. \(2024\)](#).

Let us consider the observable  $\phi$  from (23) for some subnetwork  $C$  and a variation in the data distribution as in (10) for some  $q'$ . Substituting this observable into (37), we denote the result by

$$\chi(w^*; C, q') = -\langle \phi \Delta L; w^*, C \rangle_\beta + \langle \phi; w^*, C \rangle_\beta \langle \Delta L; w^* \rangle_\beta + O\left(\frac{1}{n}\right) \quad (40)$$

where  $\langle -; w^*, C \rangle_\beta$  denotes an expectation defined as in [Wang et al. \(2024\)](#) where we fix the parameters  $u = u^*$ . To explain: the  $\delta(u - u^*)$  in  $\phi$  means that the expectations involving  $\phi$  are computing an integral over the *weight-refined* posterior, where only parameters in the circuit  $C$  (represented by the variables  $v$ ) are allowed to vary. However the expectation  $\langle \Delta L; w^* \rangle_\beta$  is defined with respect to the “full” posterior, where all parameters are allowed to vary.

If we let  $\{w_t\}_{t=1}^r$  denote approximate samples from the weight-refined posterior for  $C$  (that is, the same kind of samples we would use to define the *weight-refined* but *not* also data-refined LLC) and let  $\{w'_t\}_{t=1}^r$  denote approximate samples from the full posterior (the kind of samples we would use to define the ordinary LLC) then the susceptibility is

$$\begin{aligned} \hat{\chi}(w^*; C, q') &= -\frac{1}{r} \sum_{t=1}^r \left[ \{L_n(w_t) - L_n(w^*)\} \Delta L_n(w_t) \right] \\ &\quad + \frac{1}{r^2} \left[ \sum_{t=1}^r \{L_n(w_t) - L_n(w^*)\} \right] \left[ \sum_{t=1}^r \Delta L_n(w'_t) \right] \\ &= -\frac{1}{r} \sum_{t=1}^r \left[ \{L_n(w_t) - L_n(w^*)\} \{L_n^{\delta h}(w_t) - L_n(w_t)\} \right] \\ &\quad + \frac{1}{r^2} \left[ \sum_{t=1}^r \{L_n(w_t) - L_n(w^*)\} \right] \left[ \sum_{t=1}^r \{L_n^{\delta h}(w'_t) - L_n(w'_t)\} \right]. \end{aligned} \quad (41)$$

### 3.2 Per-Token Susceptibility

Consider a small mixing ratio  $\delta h = \frac{m}{n}$  with samples  $D_n^0 = \{(x_i, y_i)\}_{i=1}^n$  from  $q$  and samples

$$D_n^{\delta h} = \{(x'_i, y'_i)\}_{i=1}^m \cup \{(x'_i, y'_i)\}_{i=m+1}^n$$

where  $(x'_i, y'_i) \sim q'$  for  $1 \leq i \leq m$  and  $(x'_i, y'_i) \sim q$  for  $m+1 \leq i \leq n$ . Then with

$$\ell_{(x,y)}(w) = -\log p(y|x, w),$$

we have as functions of  $w$

$$\begin{aligned} \Delta L_n &= L_n^{\delta h} - L_n \\ &= \frac{1}{n} \left[ \sum_{(x',y') \in D_n^{\delta h}} \ell_{(x',y')} - \sum_{(x,y) \in D_n^0} \ell_{(x,y)} \right] \\ &= \frac{\delta h}{m} \left[ \sum_{i=1}^m \{\ell_{(x'_i, y'_i)} - \ell_{(x_i, y_i)}\} + \sum_{i=m+1}^n \{\ell_{(x'_i, y'_i)} - \ell_{(x_i, y_i)}\} \right]. \end{aligned} \quad (42)$$

The second summand inside the brackets has zero expectation over the data distribution, since the samples involved all come from  $q$ . In particular, it does not depend on  $q'$ , and so while this random variable could have nonzero covariance with  $\phi$ , the interesting information in the susceptibility comes from the first summand, which we can write as

$$\delta h \cdot \frac{1}{m} \sum_{i=1}^m \left[ \ell_{(x'_i, y'_i)} - L_m \right], \quad (43)$$

where  $L_m(w)$  is an empirical loss for the data distribution  $q$ .

**Definition 3.2.** Given a token sequence  $x$  and token  $y$ , the *per-token susceptibility* is

$$\chi_{(x,y)} := -\text{Cov}_\beta \left[ \phi, \ell_{(x,y)}(w) - L(w) \right]. \quad (44)$$

Sometimes we abuse notation and refer to the per-token susceptibility for  $y$ .

The estimated per-token susceptibility  $\hat{\chi}_{(x,y)}$  is defined by replacing in (41) the  $L_n^{\delta h} - L_n$  terms in each line by  $\ell_{(x,y)} - L_m$ . In our experiments we further replace  $L_m$  by  $L_n$  for computational efficiency. Note that by bilinearity and ignoring the second summand in (42),

$$\hat{\chi} \approx -\delta h \cdot \frac{1}{m} \sum_{i=1}^m \text{Cov}_{\beta} \left[ \phi, \ell_{(x'_i, y'_i)}(w) - L_m(w) \right] = \delta h \cdot \frac{1}{m} \sum_{i=1}^m \chi_{(x'_i, y'_i)}. \quad (45)$$

That is, if we average the per-token susceptibilities and multiply by  $\delta h$  we should get an approximation of the overall estimated susceptibility. This provides a natural form of *attribution* of the susceptibility to particular tokens from the probe distribution  $q'$ .

### 3.3 Joint Trajectory PCA

Trajectory Principal Component Analysis (PCA), originally developed in molecular biology (Amadei et al., 1993), provides a framework for analyzing the developmental dynamics of neural networks. We adapt a multi-trajectory variant of this technique (Briggman et al., 2005) to study how the behaviors of attention heads in our small language model evolve with respect to different data distributions. The same technique was used in Carroll et al. (2025, §4.2) to study transformers trained to do in-context linear regression.

**Constructing the data matrix.** For each attention head  $j \in \mathcal{H}$  and each dataset  $d \in \mathcal{D}$ , we measure the susceptibility  $\chi_j^d(t)$  at each training checkpoint  $t \in \mathcal{T}$ . This gives us, for each dataset  $d$ , a trajectory through a space with dimensions corresponding to attention heads:

$$\gamma_d(t) = (\chi_1^d(t), \chi_2^d(t), \dots, \chi_{|\mathcal{H}|}^d(t)) \in \mathbb{R}^{|\mathcal{H}|}. \quad (46)$$

We combine these trajectories into a data matrix  $X \in \mathbb{R}^{|\mathcal{D}||\mathcal{T}| \times |\mathcal{H}|}$  where each row represents the susceptibility measurements across all attention heads for a specific dataset at a specific checkpoint. For each  $d \in \mathcal{D}$ , we aggregate the row vectors from each checkpoint into a matrix  $X_d \in \mathbb{R}^{|\mathcal{T}| \times |\mathcal{H}|}$  and then stack each  $X_d$  vertically into  $X \in \mathbb{R}^{|\mathcal{D}||\mathcal{T}| \times |\mathcal{H}|}$ :

$$X_d = \begin{bmatrix} \gamma_d(t_1) \\ \gamma_d(t_2) \\ \vdots \\ \gamma_d(t_{|\mathcal{T}|}) \end{bmatrix} \text{ for } d \in \mathcal{D}, \quad X = \begin{bmatrix} X_{d_1} \\ \vdots \\ X_{d_{|\mathcal{D}|}} \end{bmatrix}.$$

**Dimensionality reduction.** We standardize each column of  $X$  to have zero mean and unit variance, ensuring that attention heads with larger susceptibility magnitudes do not dominate the analysis. Let  $X_{\text{std}}$  denote this standardized matrix. We then perform singular value decomposition (SVD)

$$X_{\text{std}} = U \Sigma V^T \quad (47)$$

where  $U \in \mathbb{R}^{|\mathcal{D}||\mathcal{T}| \times c}$  contains the left singular vectors,  $\Sigma \in \mathbb{R}^{c \times c}$  is a diagonal matrix of singular values, and  $V \in \mathbb{R}^{c \times |\mathcal{H}|}$  contains the right singular vectors where  $c$  is the chosen number of principal components. The principal components are given by the columns of  $U \Sigma$ , and the loadings that indicate how attention heads contribute to each principal component are given by the rows of  $V^T$ . The matrix decomposition (47) is one way to attempt to recover the underlying modes of the data distributions, or at least a coarse-graining of them, following the theoretical prescription in (35). In this interpretation, the right singular vectors tell us about the relationship between attention heads and modes, and the principal components tell us about the coupling between modes and datasets.

**Trajectory projection.** For each dataset  $d$ , we project its trajectory  $\gamma_d(t)$  onto the reduced space defined by the first  $k$  principal components  $\pi_d(t) = (\gamma_d(t) - \mu) \cdot V_k$  where  $\mu$  is the mean vector used during standardization and  $V_k$  consists of the first  $k$  columns of  $V$ . This gives us a low-dimensional representation  $\pi_d(t) \in \mathbb{R}^k$  of the trajectory for dataset  $d$  at checkpoint  $t$ .

## 4 Results

Following Elhage et al. (2021), Olsson et al. (2022), Hoogland et al. (2025) and Wang et al. (2024) we study two-layer attention-only (without MLP layers) transformers trained on next-token prediction

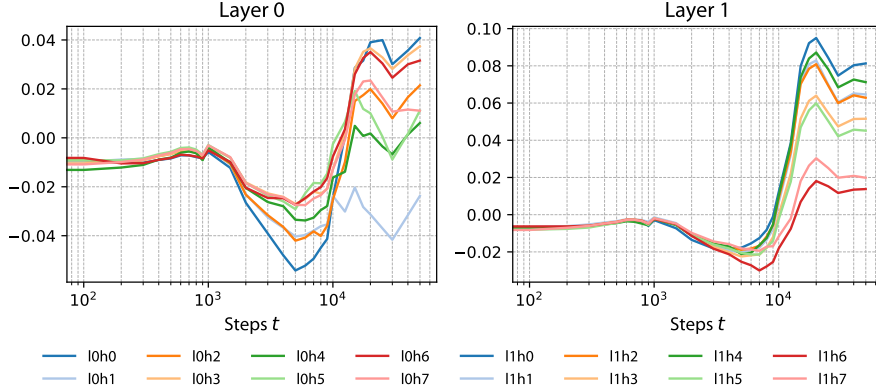


Figure 3: github susceptibilities for each head over training.

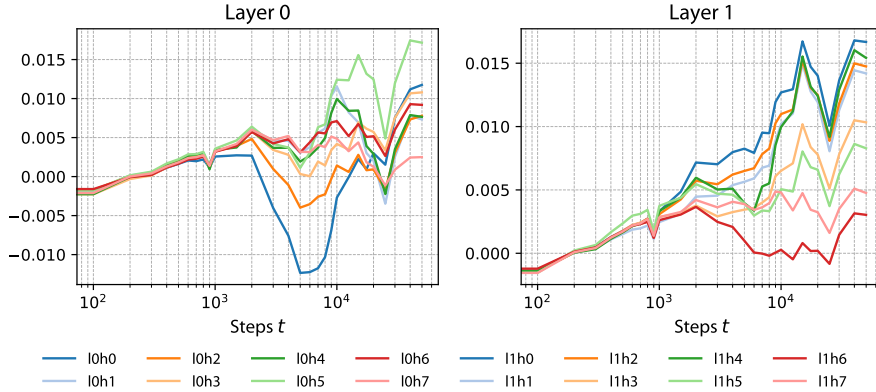


Figure 4: freelaw susceptibilities for each head over training.

on a subset of the Pile (Gao et al., 2020; Xie et al., 2023). For architecture and training details see Hoogland et al. (2025). Throughout, we refer to attention head  $h \in \{0, \dots, 7\}$  in layer  $l \in \{0, 1\}$  by the notation  $(l:h)$ .

We denote an input context, a sequence of tokens  $t_k$ , by  $S_K = (t_1, \dots, t_K)$  where  $K$  is the context length. We denote by  $S_{\leq k}$  the sub-sequence  $(t_1, \dots, t_k)$  of  $S_K$ . Our data  $D_n$  is a collection of length- $K$  contexts,  $\{S_K^i\}_{i=1}^n$ , from a data distribution  $q$ , indexed by the superscript  $i$ .

The empirical loss with respect to  $D_n$  is

$$L_n(w) = -\frac{1}{n} \sum_{i=1}^n \frac{1}{K-1} \sum_{k=1}^{K-1} \log(\text{softmax}(f_w(S_{\leq k}^i))[t_{k+1}^i]), \quad (48)$$

where for a probability distribution  $P$  over tokens we denote by  $P[t]$  the probability of token  $t$ , and  $f_w$  is the function from contexts to probability distributions of next tokens computed by the transformer. The corresponding population loss  $L(w)$  is defined by taking the expectation with respect to the true distribution of contexts.

#### 4.1 Susceptibilities Vary Across Datasets and Heads

The purpose of measuring susceptibilities is to use these “responses” to external perturbations in the data distribution to infer internal structure. Thus the first test for the methodology is whether or not the set of perturbations that we are using (here associated to Pile subsets) elicits a sufficient variety of responses. To argue for this we plot in Figure 3-Figure 5 susceptibilities for three Pile subsets github, freelaw, hackernews across training checkpoints.

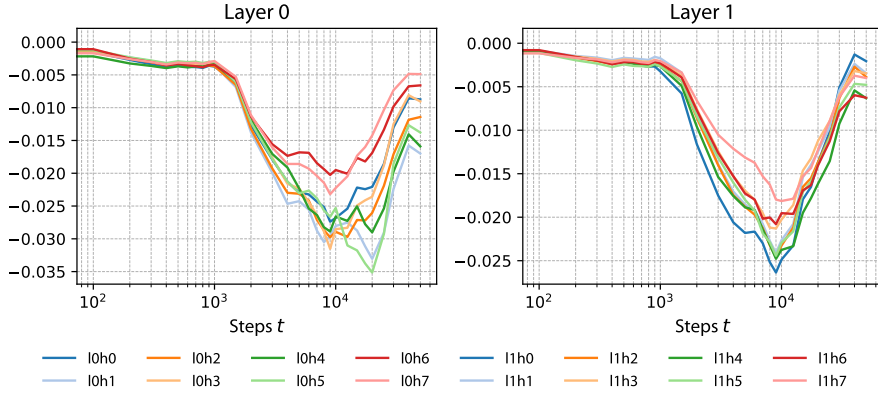


Figure 5: hackernews susceptibilities for each head over training.

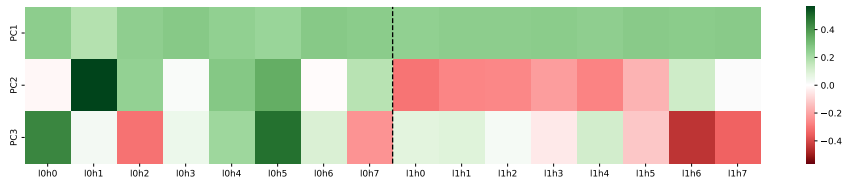


Figure 6: **Loadings of PCs on heads.** The loadings of each principal component on each head is shown, with the first principal component being a uniform mode, the second principal component loading (in layer 1) on the multigram circuit, and the third principal component loading on the induction heads and (1:5).

Note that by definition the susceptibility with respect a variation of the Pile  $q$  in the direction of a Pile subset  $q'$  is zero if  $q'$  is distributed identically to  $q$ . Thus for subsets that are similarly distributed to the overall Pile we should expect susceptibilities to be small.

Some observations from these figures:

- Susceptibilities can be both positive and negative: most values for `github`, `freelaw` are positive at the end of training (with the exception of (0:1) on `github`, which we will return to later in more detail). However *all* heads have negative susceptibility for `hackernews` at the end of training.
- In `github`, `freelaw` we see a greater variation among the heads than we do in `hackernews`, particularly in layer 1.
- The overall shapes of the susceptibility curves are quite different across datasets, for example  $t = 10^4$  seems to be an important developmental milestone in `github`, `hackernews` but not in `freelaw`.

A less subjective picture of the variation across datasets can be found in Figure 14.

It seems clear from this data (for all Pile subsets see Appendix D) that there is significant variation in susceptibilities across datasets and heads, so susceptibilities contain some information. The next question is whether or not this information is *accessible*: that is, can we understand *what* changes in the data distribution are responsible for the variation in the susceptibilities? This question is addressed in the next section.

## 4.2 Trajectory PCA

The idea of structural inference based on susceptibilities (Section 2.5) is that internal computational structures in models are the latent variables that couple *changes in the data distribution* to *changes in expectation values of observables* (i.e. susceptibilities). To test this hypothesis in our small language

model we perform joint trajectory PCA (Section 3.3) as a concrete realisation of the structural inference proposed in Section 2.5.

We found that three principal components explained 98% of the variance (Figure 13). We see that the first principal component is a uniform mode. Before describing the remaining PCs we recall from Wang et al. (2024) that we found a broad classification of the heads in this model as follows:

- [0:1](#), [0:4](#) are previous-token heads, [0:5](#) is a current-token attention head, and the rest of the layer 0 heads appeared to be mostly involved in multigram prediction, so we referred to them as multigram heads.
- [1:6](#), [1:7](#) are induction heads, [1:0-1:5](#) are multigram heads. We noted that [1:6](#) seemed somewhat specialized to induction patterns in code. Here an induction pattern means `A B ... A B` for arbitrary tokens `A`, `B`.

This classification was based on ablation studies; see (Wang et al., 2024, Appendix B).

We also noted that there appears to be coordination between layer 0 multigram heads and [1:5](#) to predict matching nested brackets, and more broadly a *multigram circuit* where layer 0 multigram heads and layer 1 multigram heads compose. Here by a *circuit* we mean a set of heads that appear to coordinate in some fashion, as measured by ablation scores, K-composition scores or other metrics Elhage et al. (2021). The induction circuit in this model, observed already in Hoogland et al. (2025) involves K-composition between [0:1](#), [0:4](#) and the induction heads [1:6](#), [1:7](#).

We had noted in Wang et al. (2024, §4.2) that relative to the LLCs computed on the full Pile computing LLCs with the data distribution `github` had a different effect on layer 1 multigram heads to the induction heads. We also noted that using a data-distribution generated by a 1-layer model (which we presume “only knows multigrams”) separated the layer 1 multigram heads from the rest of the heads in the model. These experiments, which aimed to differentially affect heads based on their sensitivity to different kinds of patterns in the data distribution, were the precursors of the present work.

Now let us turn to the PCs in Figure 6:

- **PC2** loads strongly positively on [0:1](#) and negatively on [1:0-1:5](#), that is, the layer 1 multigram heads.
- **PC3** loads strongly positively on [0:0](#), [0:5](#) and negatively on [0:2](#), [0:7](#) in layer 0 and strongly negatively on [1:6](#), [1:7](#) in layer 1.

It is not clear how to read the involvement of the layer 0 heads in these PCs, but it is quite striking that PC2 picks out the layer 1 heads involved in the multigram circuit from Wang et al. (2024) and PC3 picks out the layer 1 heads involved in the induction circuit. Given the aforementioned results, this is of course not completely surprising: we had already demonstrated in Wang et al. (2024) that varying the data distribution could be used to separate these sets of heads. Nonetheless, here the separation is done in a completely unsupervised manner and is more systematic. Additional plots can be found in Appendix B.

### 4.3 Comparison of Susceptibilities with Losses

Another important question is whether susceptibilities are really *new* information; in particular, do they provide different information to losses or ablations. In Figure 7 we show that this is the case. We select a pair of attention heads [0:0](#), [1:2](#) and a pair of datasets `github`, `dm_mathematics` and for data sampled from each dataset we compute the pair  $(s, a)$  where  $s$  is the per-token susceptibility and  $a$  is the loss after ablation minus the pre-ablation loss (we call this the *ablation delta*). The correlation between these two metrics is very small.

Under the presumption that ablations and susceptibilities are both valid techniques for inferring facts about internal structure in models, they must often arrive at the same *conclusions*, which are facts about the model independent of any technique. Indeed, in Section 4.2 we noted that structural inference based on susceptibilities seems to arrive at similar conclusions to those in Wang et al. (2024) which were partly based on ablations.

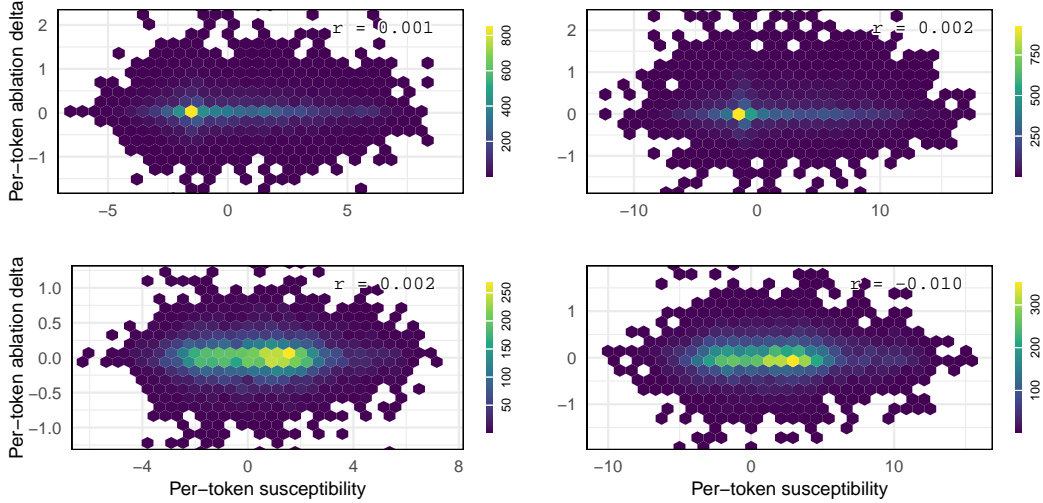


Figure 7: **Susceptibilities vs ablations.** Each plot shows distributions of per-token susceptibilities versus zero ablation loss differences as density maps. Each subplot corresponds to a pair of attention head and Pile subset, with datasets fixed across rows (top: github, bottom: dm\_mathematics) and heads fixed across columns (left: 0:0, right: 1:2). Hexagon colors indicate a count of tokens with susceptibility and ablation delta values in a given region. Shown inset are the Pearson correlation coefficients, indicating negligible correlation.

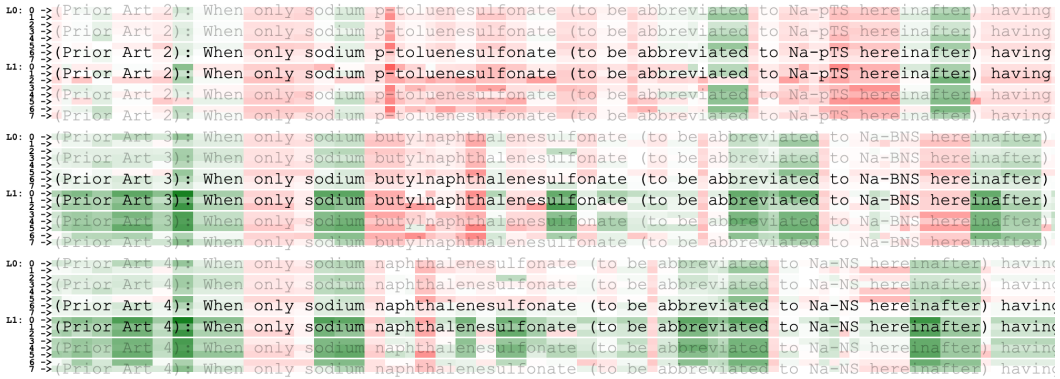


Figure 8: **Visualizing the differences across heads.** In this context sampled from uspto\_backgrounds the beginning of three lines are shown. Each line is repeated six times, and each repeat is divided into three color bars. These bars correspond to individual heads, as shown on the left, with green for positive and red for negative. The normalization is shared across all heads, so color strength is proportional to susceptibility value.

#### 4.4 Per-token Susceptibilities Vary with Context Length

We often observe that the per-token susceptibilities of layer 0 heads do not change much as a function of context length, whereas the changes are larger for layer 1 heads. For example, layer 1 heads often show increases in susceptibility for subsequent instances of repeated token sequences. An example of this phenomena is given in Figure 8.

Our interpretation of this observation is that layer 1 heads are, by virtue of being able to receive inputs from layer 0 heads, able to compute more complex functions of the context. Thus it is thus not surprising that their susceptibilities vary more with context. However, it is surprising that the induction heads 1:6, 1:7 do not show a stronger variation. This phenomena is addressed more systematically in Appendix G.

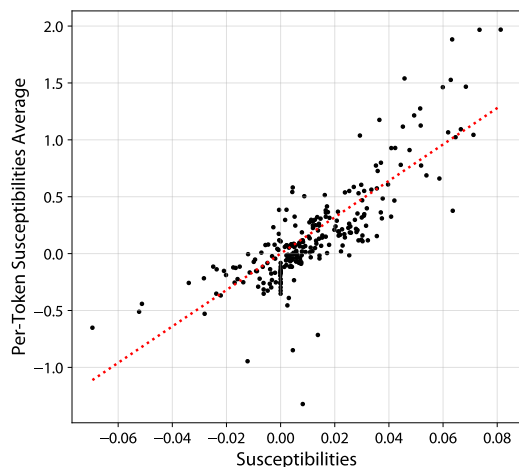


Figure 9: Comparison of average per-token susceptibilities and susceptibilities for every attention head and dataset. The dotted red line is the line of best fit.

#### 4.5 Per-token Susceptibilities Explain Susceptibility Differences

It is natural to ask *why* some heads are outliers for particular datasets but not others. For instance [0:1](#) is a negative outlier (by which we mean that it lies below the other heads) for `github` but not `freelaw` or `hackernews`. Based on Section 2.4 our model for susceptibilities is that a head is sensitive to some patterns in the data distribution more than others (we say it is *susceptible* to the pattern) and as we vary the data distribution this will drive different responses from different heads.

On this basis our hypothesis is that [0:1](#) is negatively susceptible to a pattern that is common in `github` but not in the other two datasets. To explore this we turn to the per-token susceptibilities (Definition 3.2) which we use to explain differences in overall susceptibilities. For this to be a sound methodology we need the averaged per-token susceptibilities to co-vary correctly with the susceptibility. In Figure 9 we plot one against the other. The Pearson’s correlation coefficient is 0.817 and the line of best fit has slope 15.992. Since  $\delta h = 0.1$  we would predict that the slope should be 10. We view this as sufficiently well-correlated that we can use per-token susceptibilities to address *coarse, large-scale* differences between susceptibilities in plots like Figure 3-Figure 5.

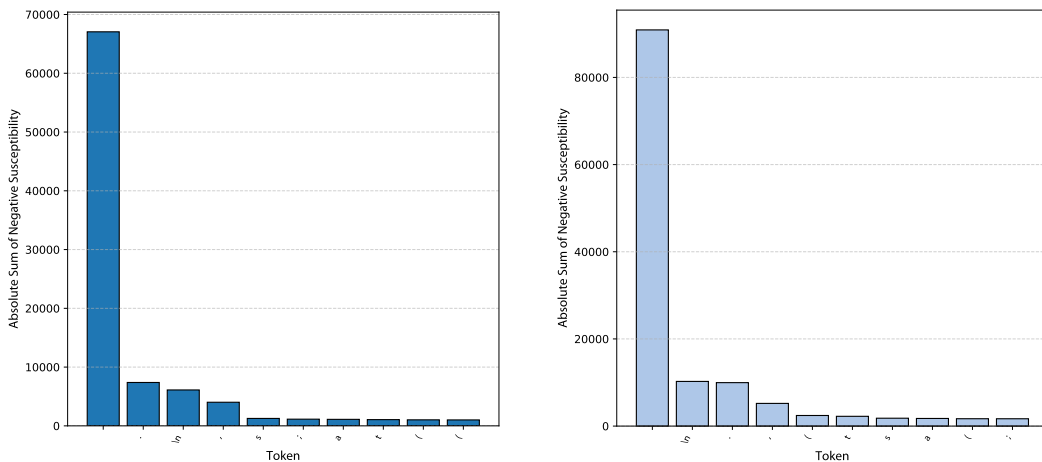


Figure 10: **Top negative susceptibility tokens.** Shown is the overall sum of negative susceptibility magnitude from 163k tokens sampled from `github-all`. *Left:* [0:0](#), *Right:* [0:1](#). In both cases the top contributing token is a space .

Let us now turn to a detailed study of `0:0` versus `0:1` on github (at the end of training). For 163k tokens sampled from github-all we form the data in Table 1. Note that to obtain the scaled sum we add up the total positive and total negative susceptibility, compute the average over tokens by dividing by 163,840, and then multiply by  $\delta h = 0.1$  (see (45)).

Head	Total pos.	Total neg.	Sum	Scaled sum	Mean	Std
<code>0:0</code>	167,995	-150,179	17,816	0.01	-1.57	0.52
<code>0:1</code>	134,362	-220,921	-86,559	-0.05	-2.13	0.76

Table 1: Total negative and positive per-token susceptibility for two attention heads on github-all and statistics for per-token susceptibilities  $\chi_{(x,y)}$  with  $y = \text{█}$  the space token.

Comparing to the actual overall susceptibilities in Figure 3 we see that `0:0` is around 0.04 and `0:1` is below  $-0.02$ , so the scaled sums are not very accurate. However they do have the right sign and the gap of  $\approx 0.06$  is correct. The gap in total positive per-token susceptibility is 34k vs a gap of 71k in the negative susceptibility. Since we want to understand why `0:1` is a negative outlier, we focus on the latter gap. In Figure 10 we show the total contributions of individual tokens  $y$  (over all contexts  $x$ ) to the total negative susceptibility for the two heads. In both cases we see that the bulk comes from the space token `█`, which contributes roughly an order of magnitude more than the next most important token. In fact `█` accounts for 45% of the total negative susceptibility for `0:0` and 41% for `0:1`. The space token appears 42,764 times in this dataset, and the statistics of the per-token susceptibilities for `█` (in any context) are shown in Table 1. The full distributions are shown in Figure 35 of Appendix G.1.

The difference in the means is enough to explain about 24k of the total 71k gap in negative susceptibility, so about a third. This is evidence that the reason `0:1` is a negative outlier on github-all is that this head is substantially more susceptible to the space token than other heads (e.g. it is 36% larger in magnitude than the mean susceptibility of `0:0`) and spaces are more frequent in github than freelaw or hackernews (compare 43k occurrences for github with 32k for freelaw and 16k for hackernews). This is not surprising since code is often structured using space tokens.

#### 4.6 Bimodal Tokens

The per-token susceptibility  $\chi_{(x,y)}$  is a function of a context  $x$  and an individual token  $y$  being predicted in that context. In Section 4.5 we saw how differences in susceptibilities of heads can potentially be attributed to per-token susceptibilities, but there the analysis was of a token  $y = \text{█}$  independent of its context  $x$ . Since not all occurrences of  $y$  are semantically the same, we should expect that the distribution of susceptibilities across  $x$  for a fixed  $y$  should sometimes reflect this.

Indeed, in this section we report on an interesting phenomena where this distribution can be bimodal: there are some tokens  $y$  for which there are two *kinds* of contexts  $x$  with the susceptibilities  $\chi_{(x,y)}$  in each context clustering around well-separated values.

**The head `0:0` and token `to`.** On both github-all and arxiv we observe that the token `to` is bimodal for the attention head `0:0`, as shown in Figure 11. On arxiv there is one mode with positive susceptibility and another with negative susceptibility. A typical negative instance is

app ears `to` be relative ly ins ens itive

where the overset number is the susceptibility of the outlined token. A typical instance of the negative mode is

\$ N \ \code{to} \ \ in \ ft \ y \ \$ \ al \ ong \ .

That is, the examples in the positive mode are normal occurrences of `to` as a word, whereas the negative mode consists of occurrences that are part of LaTeX commands. For github-all the token is also bimodal, with one positive mode and a negative mode. Typical instances of the positive mode are again occurrences of `to` in normal English sentences and a typical negative instance is

if \ ( \ by \ tes \ \code{to} \ \ \_ \ s \ k \ ip \ = \ = \ - \ 1 \ ) \ .

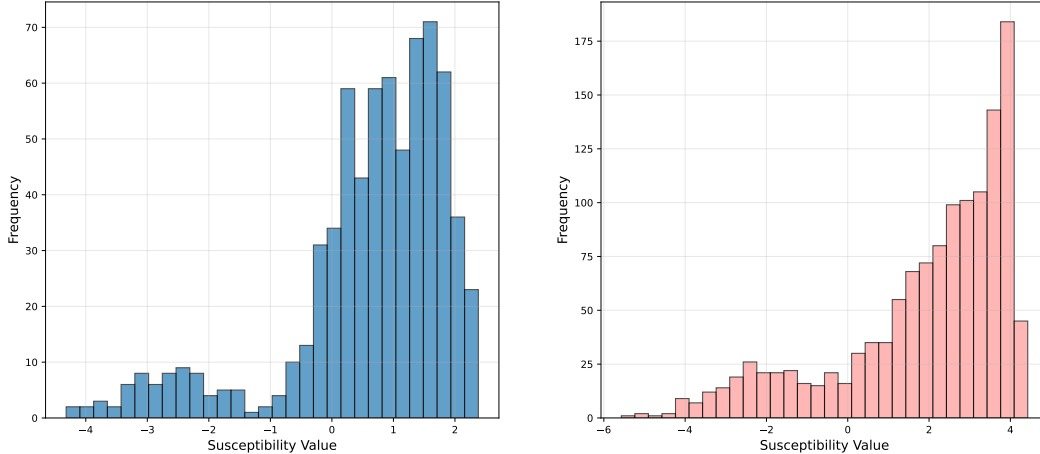


Figure 11: **Bimodal tokens.** Histograms showing frequency of certain susceptibility values for particular tokens and heads in particular datasets. *Left:* Attention head [0:0](#) and token `to` in arxiv. *Right:* Attention head [1:7](#) and token `/` in hackernews.

**The head [1:7](#) and token `/`.** Similarly we see in Figure 11 a positive and negative mode in the distribution of susceptibility values for [1:7](#) and the token `/` in hackernews. A typical instance of the positive mode is a forward slash in a URL:

n pr . org  $\left(\frac{4.10}{/}\right)$  se ctions  $\left(\frac{2.35}{/}\right)$

while typical negative instances are “either/or” constructions

sa ving  $\left(\frac{-2.76}{/}\right)$  com m itting , has h ic or p  $\left(\frac{-3.61}{/}\right)$  go - m mult ier ror .

Interestingly the distribution of susceptibilities is also bimodal for the same head and token on enron\_emails, with the positive mode still being about slashes in URLs, but the negative mode is closer to zero and occurs much more frequently (see Figure 36). Typical negative instances are

K ay M ann  $\left(\frac{-2.73}{/}\right)$  C or p  $\left(\frac{-1.12}{/}\right)$  En ron , 11  $\left(\frac{-0.33}{/}\right)$  09  $\left(\frac{1.60}{/}\right)$  2 000 .

## 5 Related Work

**Ablations and mechanistic interpretability.** One way to think about susceptibilities is that we measure correlations of various changes in losses that result from perturbing the weights in a particular part of the network. A similar, but much more extreme, perturbation is performed by ablation techniques. These are widely used in mechanistic interpretability to test hypotheses about the computation being performed by parts of neural networks (Chan et al., 2022; Wang et al., 2023; Rauker et al., 2023; Bereska and Gavves, 2024). By performing these interventions and observing the change in losses, researchers aim to infer facts about internal structure. In this paper we compare susceptibilities to zero ablation (Meyes et al., 2020; Hamblin et al., 2023; Nanda et al., 2023; Morcos et al., 2018; Zhou et al., 2018).

**Influence functions as a special case.** Classical influence functions measure the effect of up-weighting one training example on an estimator (Cook and Weisberg, 1980; Koh and Liang, 2017). Let us sketch the relation of susceptibilities to the Bayesian form of influence functions. Suppose we have a dataset  $D_n = \{(x_i, y_i)\}_{i=1}^n$ . We introduce a single new sample  $(x_{\text{new}}, y_{\text{new}})$  into the likelihood with a (small) inverse-temperature parameter  $h$  controlling how “strongly” this new sample is weighted. Concretely, we replace the posterior by

$$p(w|D_n, h) = \frac{1}{Z_{n,h}} \exp\{-nL_n(w)\} \exp\{-h\ell(w; x_{\text{new}}, y_{\text{new}})\} \varphi(w),$$

where  $\ell(w; x_{\text{new}}, y_{\text{new}})$  is the negative log-likelihood on the new sample. Next we fix a test point  $(x_{\text{test}}, y_{\text{test}})$  and define an observable  $\phi(w) = \ell(w; x_{\text{test}}, y_{\text{test}})$ . Then it is easy to check that

$$\chi = -\text{Cov}_{p(w|D_n)}[\ell(w; x_{\text{test}}, y_{\text{test}}), \ell(w; x_{\text{new}}, y_{\text{new}})] \quad (49)$$

is the covariance of the two per-sample losses with respect to the unperturbed posterior. Thus influence functions, in this sense, are a special case of susceptibilities. However, in this paper we focus on a different special case, where the observables are tied to parts of the model and the perturbation of the posterior comes from a larger shift than the introduction of a single sample. *A priori* it is not clear, from a statistical physics point of view, how meaningful the shift in the posterior from a single example should be for a model trained on a large diverse corpus.

## 6 Discussion

**Negative versus positive.** As in physics, susceptibilities in our setting can be both positive and negative, and in practice we observe a significant semantic distinction between the kinds of tokens that appear with each polarity. This can be seen in Figure 1 where negative tokens often tend to be spaces, newlines or tabs, or other structural elements to do with space. Commonly word beginnings are negative but word endings are positive. Brackets of various kinds are typically positive.

**Spaces are tokens too.** In data distributions like the Pile, predicting spaces and other “in between” tokens is an important component of next-token prediction. Often in language model interpretability we tend to focus on *words*, but spaces, fullstops, commas and brackets are influential patterns in the susceptibilities for our small language model.

**Subtle differences in susceptibilities can have big effects.** Note that small variations in the per-token susceptibilities can lead, for common tokens, to large differences in the overall susceptibilities. In this sense the homogeneity of some of the per-token visualizations and analysis in Appendix D needs to be understood correctly; the nuances in these visualizations can represent significant variation; see Section 4.5.

**Susceptibilities as LLC derivatives.** The susceptibility can be thought of as a finite difference quotient of refined LLCs (Remark 2.9) and since the susceptibility is approximately the sum of *per-token* susceptibilities, it is reasonable to think that if  $\chi_{(x,y)} \gg 0$  for some particular sequence  $xy$  then this sequence, if included in a dataset, will tend to increase the LLC, and likewise if it is large and negative it will tend to decrease it.

### 6.1 Prospects for Structural Inference

Following Section 2.5 we view any factorization of the data matrix  $X$  as potentially revealing information about the modes of the data distribution and the internal structures that develop in response to these modes. In this context, let us interpret the loadings from Figure 6 as our matrix  $P = V^T$  of couplings between modes and heads, and Figure 12 as our matrix  $C = U\Sigma$  of couplings between modes and variations in the data distribution. We write  $\alpha$  for PC2 and  $\gamma$  for PC3, thinking of these as modes or sets of modes.

**Principal Component  $\alpha$ .** In  $P$  we find large negative entries for the multigram heads [1:0]-[1:5] corresponding to  $\alpha$ . We can interpret this as  $\chi_{\alpha,j}^{\text{pure}}$  being negative for the indices  $j$  corresponding to these heads. From Section 2.4 we recall that the pure susceptibility is negative when the subnetwork’s main role is to predict the patterns in  $\alpha$  (which here stands for some coarse-grained collection of patterns). Whatever these patterns are,  $C$  has positive entries for  $\alpha$  on `wikipedia_en` and strong negative entries on `github`, `dm_mathematics`. Recall that this means the patterns in  $\alpha$  are more common in `wikipedia_en` than the general Pile, and *less* common in `github`, `dm_mathematics`. This is all consistent with  $\alpha$  representing a range of multigrams common in natural language but uncommon in code and mathematics. Since this is the role that had already been inferred for these heads in Wang et al. (2024) based on ablations, we view this as a passing a sanity check.

**Principal Component  $\gamma$ .** In  $P$  there are large negative entries for the induction heads [1:6], [1:7] corresponding to  $\gamma$ . We can interpret this as  $\chi_{\gamma,j}^{\text{pure}}$  being negative for the indices  $j$  corresponding to these heads. This suggests that these heads have as their main role predicting the patterns in  $\gamma$ . Whatever these patterns are,  $C$  has a large *positive* entry for `dm_mathematics` and a negative entry

for `stack_exchange`. This means the patterns in  $\gamma$  are more common in `dm_mathematics` than the Pile, *less* common in `stack_exchange` and about as common in `github`.

We have already identified (1:6), (1:7) as induction heads in Hoogland et al. (2025) so it is tempting to think  $\gamma$  should in part consist of induction patterns. Indeed `dm_mathematics` is, by construction, highly repetitive with many instances of the same template, so it is objectively “rich” in induction patterns. However, if this is the case it is not obvious why there is not a higher positive loading on `github`, which also contains many induction patterns.

In any case the interpretation of  $P$  is suggestive but not completely clear, while the interpretation of  $C$  in Section 4.2 seems straightforward and recovers a picture similar to the one arrived at in Wang et al. (2024), which noted the main internal computational structures in this model to be the multigram circuit (here associated with PC2) and the induction circuit (here associated with PC3).

## 7 Conclusion

In this paper we introduced *susceptibilities*, a new technique for studying internal structure in neural networks. We explored the estimated susceptibilities for attention heads and Pile subsets in a small language model, and found that the results are non-trivial and not obviously redundant with other interpretability techniques like ablations. We demonstrated how per-token susceptibilities can be used to reason about the patterns that distinguish attention heads from one another.

With this we view the basic validation of susceptibilities as complete. In future work we will apply the technique in larger models and to perform more complex forms of structural inference. In general, we find it hopeful that there is low hanging fruit on the border of neural network interpretability and statistical physics, and we look forward to bringing the mature toolkit of susceptibility analysis from condensed matter science to the study of deep learning systems.

## References

- A. Altland and B. D. Simons. *Condensed matter field theory*. Cambridge University Press, 2010.
- A. Amadei, A. B. Linssen, and H. J. Berendsen. Essential dynamics of proteins. *Proteins: Structure, Function, and Bioinformatics*, 17(4):412–425, 1993.
- V. Balasubramanian. Statistical inference, Occam’s razor, and Statistical Mechanics on the Space of Probability Distributions. *Neural Computation*, 9(2):349–368, 1997.
- M. Bauer, M. Bruveris, and P. W. Michor. Uniqueness of the fisher-rao metric on the space of smooth densities. *Bulletin of the London Mathematical Society*, 48(3):499–506, 2016.
- L. Bereska and S. Gavves. Mechanistic Interpretability for AI Safety - A Review. *Transactions on Machine Learning Research*, 2024. URL <https://openreview.net/forum?id=ePUVetPKu6>.
- P. G. Bissiri, C. C. Holmes, and S. G. Walker. A general framework for updating belief distributions. *Journal of the Royal Statistical Society: Series B (Statistical Methodology)*, 78(5):1103–1130, 2016.
- K. L. Briggman, H. D. Abarbanel, and W. Kristan Jr. Optical imaging of neuronal populations during decision-making. *Science*, 307(5711):896–901, 2005.
- L. Carroll, J. Hoogland, M. Farrugia-Roberts, and D. Murfet. Dynamics of transient structure in in-context linear regression transformers, 2025. URL <https://arxiv.org/abs/2501.17745>.
- L. Chan, A. Garriga-Alonso, N. Goldwosky-Dill, R. Greenblatt, J. Nitishinskaya, A. Radhakrishnan, B. Shlegeris, and N. Thomas. Causal scrubbing, a method for rigorously testing interpretability hypotheses. *AI Alignment Forum*, 2022.
- Z. Chen and D. Murfet. Modes of sequence models and learning coefficients. *preprint*, 2025.
- R. D. Cook and S. Weisberg. Characterizations of an empirical influence function for detecting influential cases in regression. *Technometrics*, 22(4):495–508, 1980.

- Devin Gulliver. Monology/pile-uncopyrighted. <https://huggingface.co/datasets/monology/pile-uncopyrighted>, Mar. 2025.
- N. Elhage, N. Nanda, C. Olsson, T. Henighan, N. Joseph, B. Mann, A. Askell, Y. Bai, A. Chen, T. Conerly, N. DasSarma, D. Drain, D. Ganguli, Z. Hatfield-Dodds, D. Hernandez, A. Jones, J. Kernion, L. Lovitt, K. Ndousse, D. Amodei, T. Brown, J. Clark, J. Kaplan, S. McCandlish, and C. Olah. A mathematical framework for transformer circuits. *Transformer Circuits Thread*, 2021.
- L. Gao, S. Biderman, S. Black, L. Golding, T. Hoppe, C. Foster, J. Phang, H. He, A. Thite, N. Nabeshima, S. Presser, and C. Leahy. The Pile: an 800GB dataset of diverse text for language modeling. Preprint arXiv:2101.00027 [cs.CL], 2020.
- C. Hamblin, T. Konkle, and G. Alvarez. Pruning for Feature-Preserving Circuits in CNNs, Apr. 2023.
- J. Hoogland, G. Wang, M. Farrugia-Roberts, L. Carroll, S. Wei, and D. Murfet. Loss landscape degeneracy drives stagewise development in transformers, 2025. URL <https://arxiv.org/abs/2402.02364>.
- N. P. Jouppi, G. Kurian, S. Li, P. Ma, R. Nagarajan, L. Nai, N. Patil, S. Subramanian, A. Swing, B. Towles, C. Young, X. Zhou, Z. Zhou, and D. Patterson. Tpu v4: An optically reconfigurable supercomputer for machine learning with hardware support for embeddings, 2023. URL <https://arxiv.org/abs/2304.01433>.
- P. W. Koh and P. Liang. Understanding black-box predictions via influence functions. In *International conference on machine learning*, pages 1885–1894. PMLR, 2017.
- C. H. LaMont and P. A. Wiggins. Correspondence between thermodynamics and inference. *Physical Review E*, 99(5):052140, 2019.
- E. Lau, Z. Furman, G. Wang, D. Murfet, and S. Wei. The local learning coefficient: A singularity-aware complexity measure, 2024. URL <https://arxiv.org/abs/2308.12108>.
- R. Meyes, C. W. de Puiseau, A. Posada-Moreno, and T. Meisen. Under the Hood of Neural Networks: Characterizing Learned Representations by Functional Neuron Populations and Network Ablations. Preprint arxiv:2004.01254 [cs, q-bio], May 2020.
- A. S. Morcos, D. G. Barrett, N. C. Rabinowitz, and M. Botvinick. On the importance of single directions for generalization. In *International Conference on Learning Representations*, 2018. URL <https://openreview.net/forum?id=r1iuQjxCZ>.
- N. Nanda, J. Lieberum, and B. Barak. Progress measures for grokking via mechanistic interpretability. *arXiv preprint arXiv:2301.05217*, 2023.
- C. Olsson, N. Elhage, N. Nanda, N. Joseph, N. DasSarma, T. Henighan, B. Mann, A. Askell, Y. Bai, A. Chen, T. Conerly, D. Drain, D. Ganguli, Z. Hatfield-Dodds, D. Hernandez, S. Johnston, A. Jones, J. Kernion, L. Lovitt, K. Ndousse, D. Amodei, T. Brown, J. Clark, J. Kaplan, S. McCandlish, and C. Olah. In-context learning and induction heads. *Transformer Circuits Thread*, 2022.
- T. Rauker, A. Ho, S. Casper, and D. Hadfield-Menell. Toward Transparent AI: A Survey on Interpreting the Inner Structures of Deep Neural Networks. In *2023 IEEE Conference on Secure and Trustworthy Machine Learning (SaTML)*, pages 464–483, Los Alamitos, CA, USA, 2023. IEEE Computer Society.
- E. Urdshals and J. Urdshals. Structure development in list-sorting transformers, 2025. URL <https://arxiv.org/abs/2501.18666>.
- G. Wang, J. Hoogland, S. van Wingerden, Z. Furman, and D. Murfet. Differentiation and specialization of attention heads via the refined local learning coefficient, 2024. URL <https://arxiv.org/abs/2410.02984>.
- K. R. Wang, A. Variengien, A. Conmy, B. Shlegeris, and J. Steinhardt. Interpretability in the wild: a circuit for indirect object identification in GPT-2 small. In *The Eleventh International Conference on Learning Representations*, 2023.

- S. Watanabe. Almost all learning machines are singular. In *2007 IEEE Symposium on Foundations of Computational Intelligence*, pages 383–388. IEEE, 2007.
- S. Watanabe. *Algebraic geometry and statistical learning theory*. Cambridge University Press, 2009.
- S. Watanabe. *Mathematical Theory of Bayesian Statistics*. CRC Press, Taylor and Francis group, USA, 2018.
- M. Welling and Y. W. Teh. Bayesian Learning via Stochastic Gradient Langevin Dynamics. In *Proceedings of the 28th International Conference on Machine Learning*, 2011.
- S. M. Xie, S. Santurkar, T. Ma, and P. Liang. Data selection for language models via importance resampling. Preprint arXiv:2302.03169 [cs.CL], 2023.
- B. Zhou, Y. Sun, D. Bau, and A. Torralba. Revisiting the Importance of Individual Units in CNNs via Ablation. Preprint arXiv:1806.02891 [cs], June 2018.

Table 2: Details of the Pile (Gao et al., 2020) subset datasets used in our analysis.

Dataset	Description	Size (Rows)
<code>pile-github</code>	Code and documentation from GitHub	100k
<code>pile-pile-cc</code>	Web crawl data from Common Crawl	100k
<code>pile-pubmed_abstracts</code>	Scientific abstracts from PubMed	100k
<code>pile-uspto_backgrounds</code>	Patent background sections	100k
<code>pile-pubmed_central</code>	Full-text scientific articles	100k
<code>pile-stackexchange</code>	Questions and answers from tech forums	100k
<code>pile-wikipedia_en</code>	English Wikipedia articles	100k
<code>pile-freelaw</code>	Legal opinions and case law	100k
<code>pile-arxiv</code>	Scientific papers from arXiv	100k
<code>pile-dm_mathematics</code>	Mathematics problems and solutions	100k
<code>pile-enron_emails</code>	Corporate emails from Enron	100k
<code>pile-hackernews</code>	Tech discussions from Hacker News	100k
<code>pile-nih_exporter</code>	NIH grant applications	100k
<code>pile_subsets_mini</code>	Combined samples from all subsets	6.66k
<code>pile1m</code>	Combined samples from all subsets	1M

## A Data

The datasets we used to evaluate model performance are described in Table 2. These are generated by filtering for the first 100k rows from subsets of the uncopyrighted Pile (Devin Gulliver, 2025), which was generated by dropping copyrighted subsets from the Pile (Gao et al., 2020). Several subsets were omitted because there were too few rows to easily retrieve 100k samples.

We use two github datasets `pile-github` and `github-all`. The former is a pile subset, while the latter is `codeparrot/github-code` and is included for consistency with (Wang et al., 2024).

## B Additional PCA data

For the PCA visualizations the checkpoints used are the same ones given in Appendix C.1. In Figure 12 we visualize the principal components of the PCA by averaging over the time axis to obtain linear combinations of datasets. In Figure 13 we provide a scree plot for the analysis of the PCA. In Figure 14 we visualize the left singular vectors by projecting them onto the top two PCs. In Figure 15 we plot the principal components as time series.

---

\*All datasets are available on HuggingFace at <https://huggingface.co/collections/timaeus/datasets-pile-subsets-673a6a6c7ffc522a34ebfb0b>. These datasets are derived from The Pile (Gao et al., 2020) and specifically from the uncopyrighted version (Devin Gulliver, 2025), with cleaning performed by removing all content from the Books3, BookCorpus2, OpenSubtitles, YTSubtitles, and OWT2 subsets.

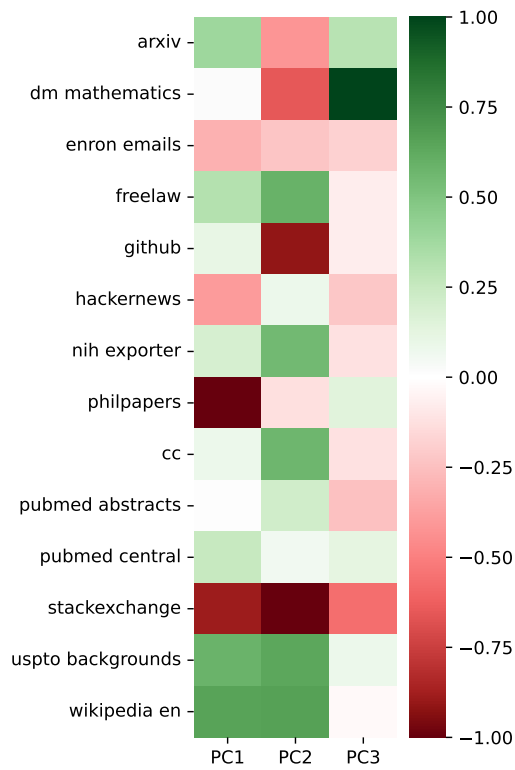


Figure 12: **Contributions of each Pile subset to PCA components.** We visualize the matrix  $U\Sigma$  from the SVD decomposition of  $X_{\text{std}}$ , with normalized columns.

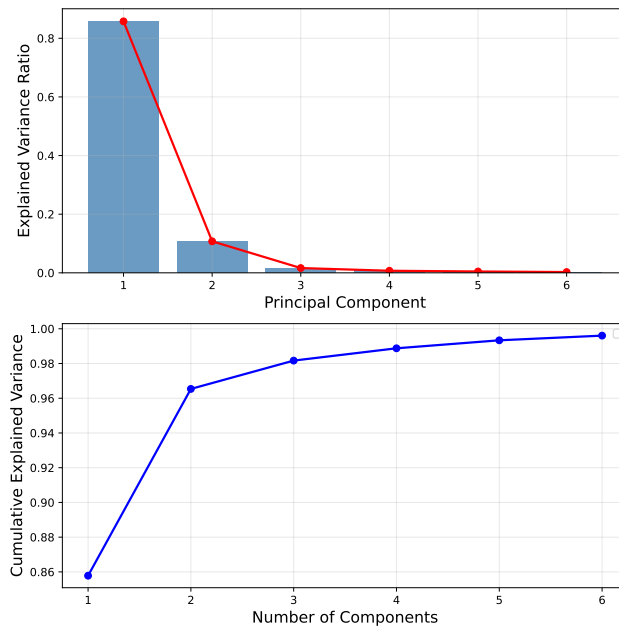


Figure 13: **Scree plot for the PCA.** We note that three principal component explain more than 98% of the variance.

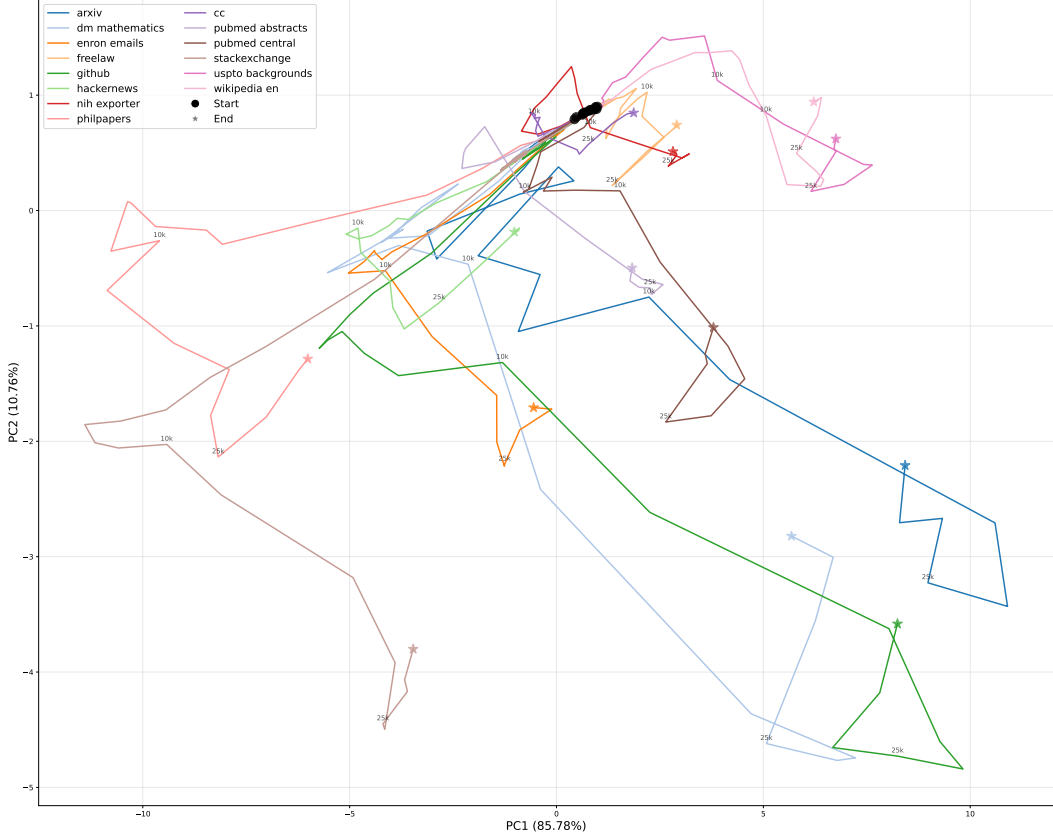


Figure 14: **The 2D projection of the time series of susceptibilities.** Using the top two PCs we project the susceptibility vector into two-dimensions. We note that the trajectories for each dataset are often distinct. Selected timesteps are shown on the trajectories.

## C Methods

### C.1 Susceptibilities

As a reminder, susceptibility estimation for the probe data distribution  $q'$  and weight restriction  $C$  is

$$\hat{\chi} = \frac{1}{r} \sum_{t=1}^r \left[ \{L_n(w_t) - L_n(w^*)\} \{L_n(w_t) - L_n^{\delta h}(w_t)\} \right] \quad (29)$$

$$- \frac{1}{r^2} \left[ \sum_{t=1}^r \{L_n(w_t) - L_n(w^*)\} \right] \left[ \sum_{t=1}^r \{L_n(w'_t) - L_n^{\delta h}(w'_t)\} \right]. \quad (30)$$

where  $w_t$  are SGLD weight samples from the weight restricted posterior,  $w'_t$  are SGLD weight samples from the full not weight restricted posterior,  $w^*$  are the initial model weights,  $L_n$  is the loss function on the pretraining dataset  $q$  on a random batch of size  $n$ , in this case  $q = \text{timaeus/dsir-pile-1m-2}$ , and  $L_n^{\delta h}$  is the loss function on a random batch of size  $n$  on  $q_{\delta h} = (1 - \delta h)q + \delta h q'$ . That is, a mixture between the pretraining dataset  $q$  and probe dataset  $q'$  using the process as specified in Appendix C.4.

These susceptibilities were found for each of the datasets listed in Appendix A, for each checkpoint step in

$$S = \{0, 100, 200, 300, 400, 500, 600, 700, 800, 900, 1000, 1500, 2000, 3000, 4000, 5000, 6000, 7000, 8000, 9000, 10000, 12500, 15000, 17500, 20000, 25000, 30000, 40000, 49900\}$$

and each attention head weight restriction, as well as no weight restriction at all. For these experiments we had a batch size of  $n = 64$ , and  $\delta h = 0.1$ . SGLD hyperparameters can be found in Appendix C.3.

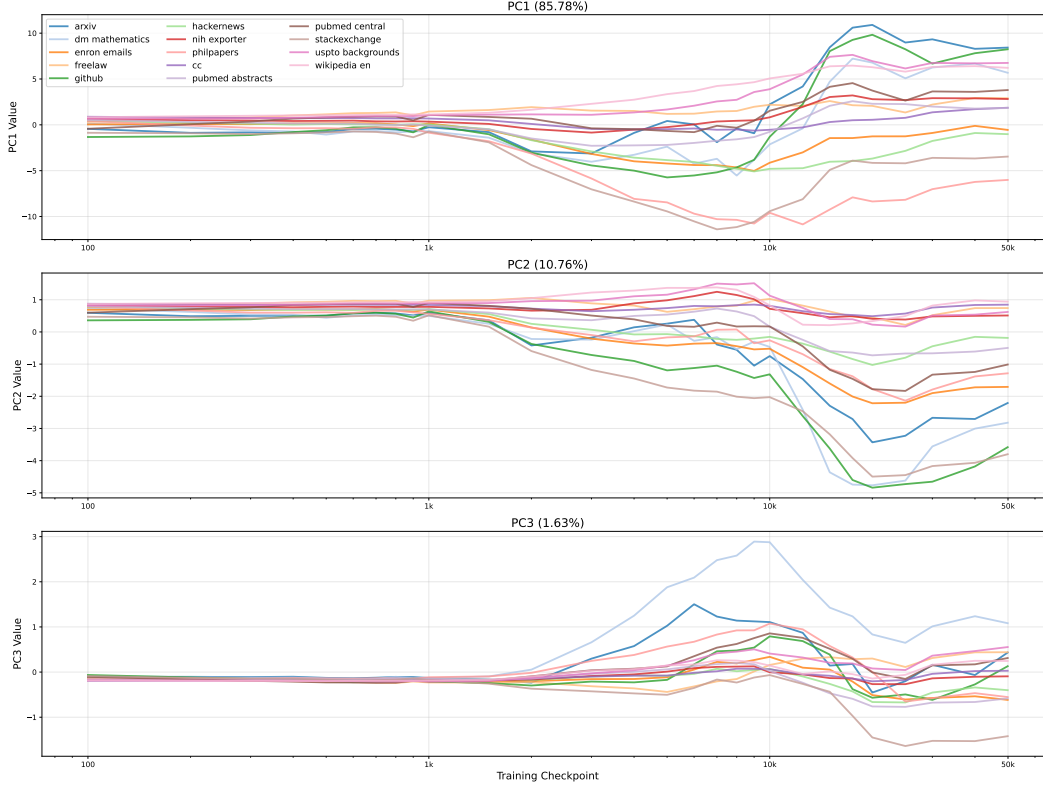


Figure 15: **The principal components as time series.** Each principal component can be interpreted as a time series for each dataset, and here we plot these against checkpoints.

The hardware used for the computation consisted of 4 TPU v4s (Jouppi et al., 2023) run in parallel, each computing the weight-refined susceptibilities of four heads, and one computing the susceptibility of the full model on every dataset for each of the 30 steps in  $S$ . This took a total of 2 hours to complete.

## C.2 Per-Token Susceptibilities

As a reminder, we estimate per-sample susceptibilities using the equation

$$\hat{\chi}_i = \frac{1}{r} \sum_{t=1}^r \left[ \{L_n(w_t) - L_n(w^*)\} \{L_n(w_t) - \ell_{(x'_i, y'_i)}(w_t)\} \right] - \frac{1}{r^2} \left[ \sum_{t=1}^r \{L_n(w_t) - L_n(w^*)\} \right] \left[ \sum_{t=1}^r \{L_n(w'_t) - \ell_{(x'_i, y'_i)}(w'_t)\} \right].$$

For a total of approximately  $M = 160 \times 1023 = 163680$  samples, across 160 different contexts, where each context  $c^r = (c_1^r, \dots, c_k^r)$  is a list of  $k \leq 1023$  tokens, with the property that for all  $j \in [2, k]$ ,  $(c_{1:j-1}^r, c_j^r) \in D_M^1$ .

We choose these contexts using the `Dataset.shuffle` method with seed 0 after tokenizing the dataset under consideration, and taking the 160 contexts.

To visualize these per-sample susceptibilities, let

$$\hat{\chi}(c_j^r) = \frac{1}{r} \sum_{t=1}^r \left[ \{L_n(w_t) - L_n(w^*)\} \{L_n(w_t) - \ell_{(c_{1:j-1}^r, c_j^r)}(w_t)\} \right] - \frac{1}{r^2} \left[ \sum_{t=1}^r \{L_n(w_t) - L_n(w^*)\} \right] \left[ \sum_{t=1}^r \{L_n(w'_t) - \ell_{(c_{1:j-1}^r, c_j^r)}(w'_t)\} \right].$$

Then this is a real number, and we can map it to a color value via either or where the only differences

---

**Require:**  $\hat{\chi}(c_j^r) \in \mathbb{R}$

- 1:  $\max(\hat{\chi}) \leftarrow \max_{r,i} |\hat{\chi}(c_j^r)|$
- 2: **if**  $\hat{\chi}(c_j^r) > 0$  **then**
- 3:      $\text{color} \leftarrow \text{rgba} \left( 0, 255, 0, \frac{|\hat{\chi}(c_j^r)|^2}{\max(\hat{\chi})} \right)$
- 4: **else**
- 5:      $\text{color} \leftarrow \text{rgba} \left( 255, 0, 0, \frac{|\hat{\chi}(c_j^r)|^2}{\max(\hat{\chi})} \right)$
- 6: **end if**

---



---

**Require:**  $\hat{\chi}(c_j^r) \in \mathbb{R}$

- 1:  $\max(\hat{\chi}) \leftarrow \max_{r,i} |\hat{\chi}(c_j^r)|$
- 2: **if**  $\hat{\chi}(c_j^r) > 0$  **then**
- 3:      $\text{color} \leftarrow \text{rgba} \left( 0, 128, 0, \frac{|\hat{\chi}(c_j^r)|}{\max(\hat{\chi})} \right)$
- 4: **else**
- 5:      $\text{color} \leftarrow \text{rgba} \left( 255, 0, 0, \frac{|\hat{\chi}(c_j^r)|}{\max(\hat{\chi})} \right)$
- 6: **end if**

---

are the shade of green and the quadratic versus linear opacity scaling.

Each  $c_j^r$  can also be decoded into a string of characters using our model’s tokenizer. Therefore we can highlight each such string the corresponding color computed above. Let  $s(c_j^r)$  be this highlighted string. Then this produces Figure 32 using the first coloring algorithm while the latter is used to produce Figure 1 and Figure 8.

For Figure 32, we sort each per-sample susceptibility in a descending manner, giving us the list  $\hat{\chi}(c_{j_1}^{r_1}) \geq \dots \geq \hat{\chi}(c_{j_M}^{r_M})$ . We then choose the first 100 of these susceptibilities, and visualize their surrounding context by concatenating each of their highlighted strings. With + denoting concatenation,

$$\begin{aligned} & s(c_{j_1-200}^{r_1}) + \dots + s(c_{j_1+200}^{r_1}) \\ & \quad \vdots \\ & s(c_{j_1-200}^{r_{100}}) + \dots + s(c_{j_1+200}^{r_{100}}) \end{aligned}$$

And we also choose the last 100 of these susceptibilities, and visualize the surrounding context in the same way

$$\begin{aligned} & s(c_{j_1-200}^{r_M}) + \dots + s(c_{j_1+200}^{r_M}) \\ & \quad \vdots \\ & s(c_{j_1-200}^{r_{M-100}}) + \dots + s(c_{j_1+200}^{r_{M-100}}) \end{aligned}$$

For Figure 1 and Figure 8, we use the same context samples from each dataset but do no sorting of the data and instead search manually for representative examples.

Here we use all the same definitions and parameters as in Appendix C.1, and SGLD sampling with hyperparameters as in Appendix C.3, modified to only use 100 draws. We run these per-token susceptibilities for all datasets in Appendix A and on checkpoint step 49900.

The hardware used for this computation consisted of a single TPU v4 (Jouppi et al., 2023), taking 3 hours in total to find the per-token susceptibilities for all heads, datasets, and tokens.

### C.3 SGLD hyperparameters

Following Wang et al. (2024) we used SGLD with hyperparameters  $\gamma = 300$ ,  $n\beta = 30$ ,  $\varepsilon = 0.001$ , batch size 64, 4 chains, and 200 draws for the regular susceptibilities as in C.1, but only 100 draws and batch size 16 for the per-token susceptibilities as in C.2.

Note that for these experiments we did not use RMSProp SGLD.

#### C.4 Dataset mixing

To create the mixed dataset  $D^{\delta h}$  consisting of samples from  $q_{\delta h} = (1 - \delta h)q + \delta h q'$ , we interleaved the pretraining dataset with each probe dataset using Algorithm 1 in order to ensure even mixing, determinacy, and the property that if  $q' = q$ , then  $D^{\delta h} = D^0$ .

Let  $(x_i, y_i)$  be samples from  $q$  and  $(x'_i, y'_i)$  be samples from  $q'$ ,

---

#### Algorithm 1 Data Mixing Algorithm

---

**Require:**  $D_N^0 = \{(x_i, y_i)\}_{i=1}^N$ ,  $D_M^1 = \{(x'_i, y'_i)\}_{i=1}^M$ ,  $\delta h \in [0, 1]$

```

1:  $D_{\min(N,M)}^{\delta h} \leftarrow \emptyset$ 
2: probe count  $\leftarrow 0$ 
3: while  $j \leq N, M$  do
4:   target probe count  $\leftarrow \lfloor (j + 1)\delta h \rfloor$ 
5:   if probe count < target probe count then
6:      $D_{\min(N,M)}^{\delta h} \leftarrow D_{\min(N,M)}^{\delta h} \cup \{(x'_j, y'_j)\}$ 
7:     probe count  $\leftarrow$  probe count + 1
8:   else
9:      $D_{\min(N,M)}^{\delta h} \leftarrow D_{\min(N,M)}^{\delta h} \cup \{(x_j, y_j)\}$ 
10:  end if
11:   $j \leftarrow j + 1$ 
12: end while

```

---

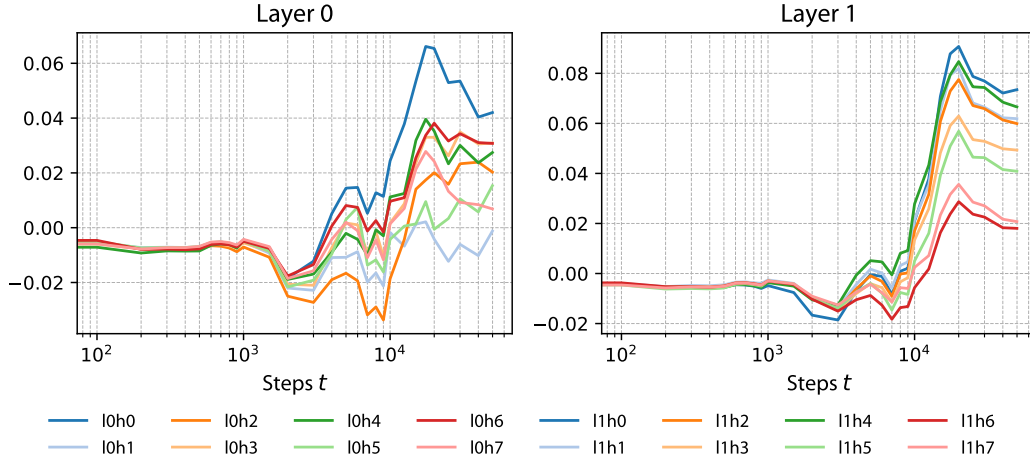


Figure 16: arxiv susceptibilities for each head over training.

## D Top Susceptibilities

In this section we give additional details for each dataset (see Appendix A).

Attention head  $h$  in layer  $l$  is denoted  $l:h$ . Tokens are denoted  $t$  and the token with high (positive or negative) susceptibility is denoted with a border like  $t$ . In this section  $x$  stands for a number token, e.g. 4, 13.

For each dataset and head we give the top three distinct high positive susceptibility tokens, in order taken from the top hundred positive susceptibility tokens found in a sample of contexts. In some cases there are two or fewer distinct tokens in the top 100 and we only list these. Note that the per-token susceptibility  $\chi(x,y)$  is a function of the predicted token  $y$  and context  $x$ . We typically only give  $y$  with at most some small segment of  $x$ , e.g. in the example

$$\overbrace{\text{wa vel}}^{\dots x_{k-1} x_k} \text{ength}$$

where only the last two tokens of the context  $x$  is given. In some cases we also show the largest magnitude negative per-token susceptibilities, with the same conventions.

In the following `://` always appears as part of `http://` or `https://` unless specified otherwise, and `####` appears as part of a “line” underneath a title or separating sections of a document. The token `=` appears as part of HTML, e.g. `class =` or similar markup.

### D.1 arxiv

The susceptibilities for each head are shown in Figure 16.

The positive susceptibilities for layer 0:

- **0:0**: wa vel ength, \ ome ga, differe nces
- **0:1**: differe nces, wa vel ength, prot ocol
- **0:2**: wa vel ength, es pecially, differe nces
- **0:3**: "=", differe nces, prot ocol
- **0:4**: wa vel ength, differe nces, prot ocol
- **0:5**: differe nces, wa vel ength, max imum
- **0:6**: "=", wa vel ength, ://

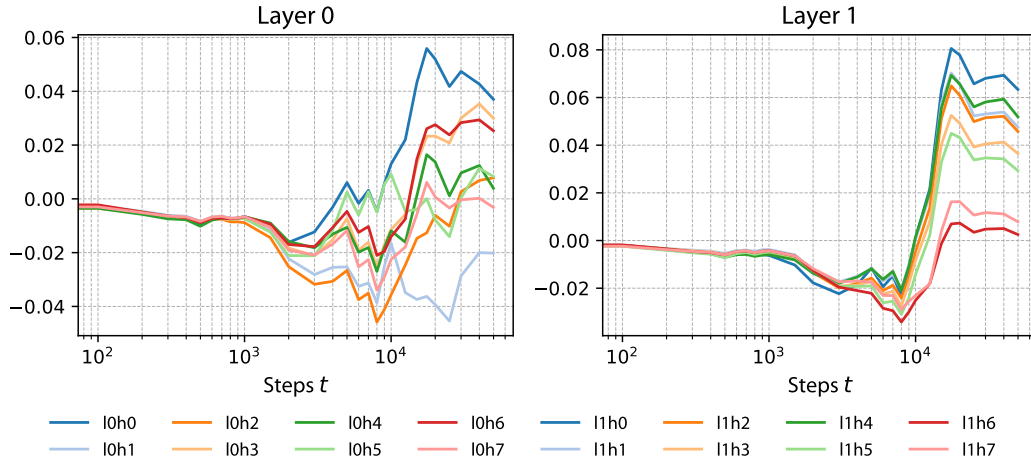


Figure 17: `dm_mathematics` susceptibilities for each head over training.

- `0:7`: `wa vel (ength), (=), mag n (itude)`

The positive susceptibilities for layer 1:

- `1:0`: `(=), wa vel (ength), \ ome (ga)`
- `1:1`: `wa vel (ength), (=), \ f (ka)`
- `1:2`: `wa vel (ength), (=), \ ome (ga)`
- `1:3`: `wa vel (ength), (=), \ ome (ga)`
- `1:4`: `wa vel (ength), \ ome (ga), mag n (itude)`
- `1:5`: `wa vel (ength), \ ome (ga), (=)`
- `1:6`: `wa vel (ength), (://), \ ome (ga)`
- `1:7`: `(=), wa vel (ength), }`

## D.2 `dm_mathematics`

The susceptibilities for each head are shown in Figure 17.

The positive susceptibilities for layer 0:

- `0:0`: `}`, `))`, `D eter (mine)`
- `0:1`: `repl ac (ement), div (ided)`
- `0:2`: `C al (cul) ate, F (alse), D eter (mine)`
- `0:3`: `F (alse), ))`, `(PM)`
- `0:4`: `repl ac (ement), C al (cul) ate, der iv (ative)`
- `0:5`: `div (ided), ter (ms), repl ac (ement)`
- `0:6`: `C al (cul) ate, D eter (mine), ))`
- `0:7`: `C al (cul) ate`

The positive susceptibilities for layer 1:

- `1:0`: `C al (cul) ate, D eter (mine)`

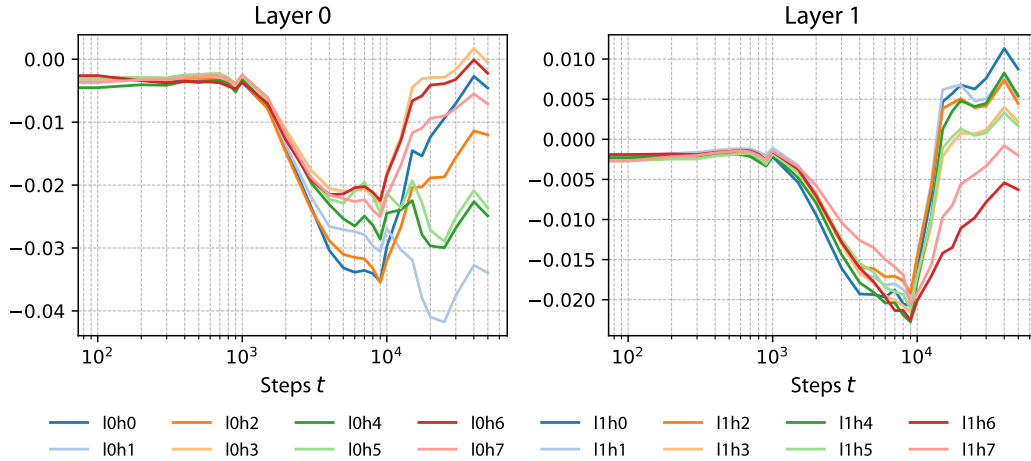


Figure 18: enron\_emails susceptibilities for each head over training.

- **1:1**: C al `cul` ate , D eter `mine`
- **1:2**: C al `cul` ate , D eter `mine` , F `alse`
- **1:3**: C al `cul` ate , D eter `mine` , F `alse`
- **1:4**: C al `cul` ate , D eter `mine` , F `alse`
- **1:5**: C al `cul` ate , D eter `mine` , F `alse`
- **1:6**: D eter `mine` , den om in `ator` , C al `cul` ate
- **1:7**: `}` , F `alse` , `)`

### D.3 enron\_emails

The susceptibilities for each head are shown in Figure 18. In the following `>` appears as part of an email tag in HTML.

The positive susceptibilities for layer 0:

- **0:0**: `####` , `://` , `=`
- **0:1**: `://` , `differe nces` , `cap ab ilities`
- **0:2**: `=` , `####` , `://`
- **0:3**: `=` , `://` , `####`
- **0:4**: `://` , `differe nces` , `=`
- **0:5**: `://` , `cap ab ilities` , `differe nces`
- **0:6**: `=` , `####` , `://`
- **0:7**: `=` , `://` , `####`

The positive susceptibilities for layer 1:

- **1:0**: `=` , `####` , `>`
- **1:1**: `=` , `####` , `>`
- **1:2**: `=` , `####` , `://`
- **1:3**: `=` , `####` , `://`

- 1:4: "=", #####, K am ins ki
- 1:5: "=", #####, >
- 1:6: ://, K am ins ki
- 1:7: "=", ://, De cember

Some remarks:

- Vincent Kaminski was head of the quantitative modelling group at Enron from 1992 until 2002.
- Since almost every occurrence http, https is followed by ://, we might expect that the model should have particularly low loss on these tokens and that this might explain why they appear so frequently in high positive susceptibility examples across the Pile subsets and in particular on enron\_emails. However, upon inspection this not appear to be the case. In Table 3 we give the per-token losses and susceptibilities for 10 occurrences of :// for 0:0. For reference the first occurrence of :// reported in the table has, in its context, per-token losses between 0.01 and 13. This is typical across the other contexts.

Index	Loss http	Loss ://	Susceptibility
1	1.07	0.15	9.06
2	0.82	0.90	8.90
3	0.32	0.01	8.74
4	1.54	11.75	8.72
5	3.08	3.06	8.72
6	3.50	12.00	8.70
7	8.63	9.19	8.69
8	0.02	0.03	8.69
9	0.56	0.28	8.67
10	4.00	0.52	8.65

Table 3: **Per-Token Loss versus Susceptibility for 0:0.** Shown are per-token losses for both tokens in the bigram and the susceptibility for just the :// token. We note the consistency of the susceptibility and the wide variations in the per-token losses.

#### D.4 nih\_exporter

The susceptibilities for each head are shown in Figure 19. Below  $x$  stands for a token representing a number.

The positive susceptibilities for layer 0:

- 0:0: (x(%)), differe nces, th y roid
- 0:1: differe nces, resear cher, ident ify
- 0:2: th y roid, ev al uate, differe nces
- 0:3: (x(%)), differe nces, ev al uate
- 0:4: differe nces, Un f ortunately, demon st ration
- 0:5: demon st ration, differe nces, th y roid
- 0:6: (x(%)), full - l ength, ev al uate
- 0:7: th y roid, Un f ortunately, full - l ength

The positive susceptibilities for layer 1:

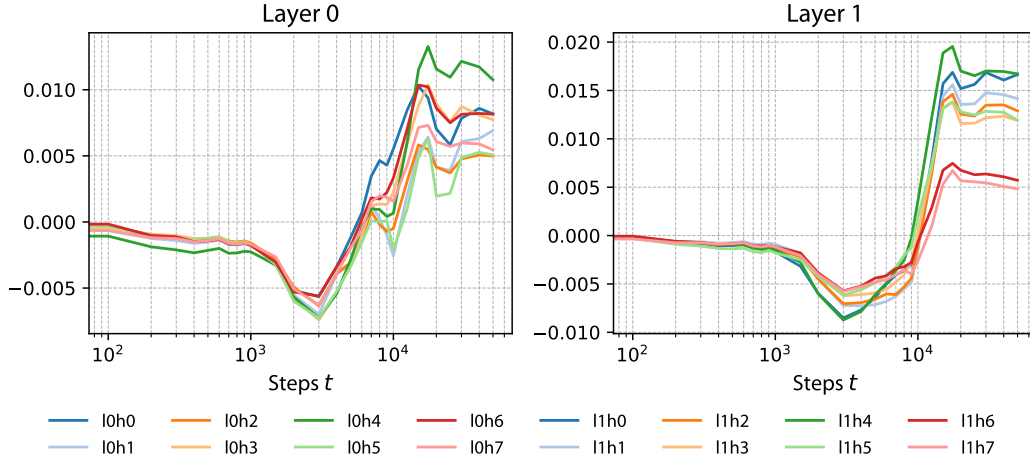


Figure 19: nih\_exporter susceptibilities for each head over training.

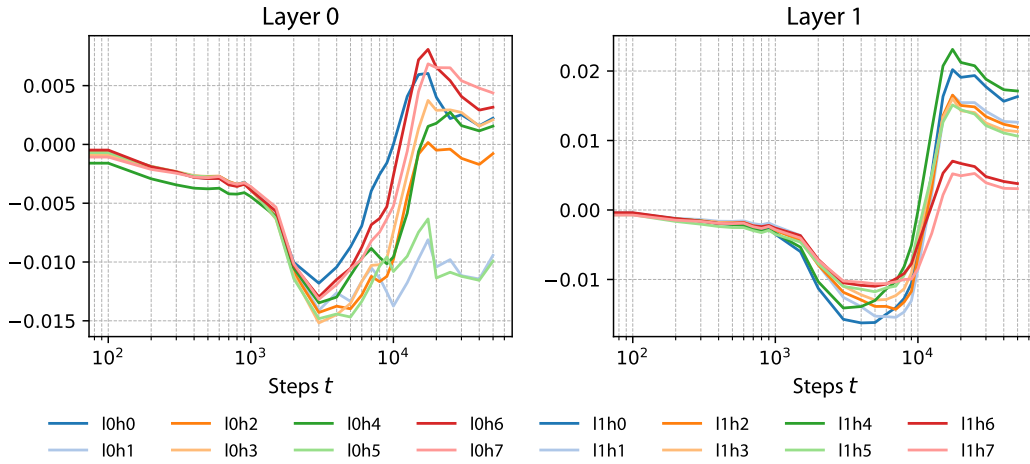


Figure 20: pubmed\_abstracts susceptibilities for each head over training.

- 1:0: ( x(%), th y (roid), prot ot (type)
- 1:1: ( x(%), ank (yr) in , F Y (09)
- 1:2: ( x(%), ant (ico) ag ul ant , (cancer)
- 1:3: ( x(%), ev al (ulate), prot ot (type)
- 1:4: th y (roid), ant (ico) ag ul ant , ( x(%)
- 1:5: th y (roid), re h ab il (itation), ant (ico) ag ul ant
- 1:6: ev al (ulate), prot (ocol), re h ab il (itation)
- 1:7: Un f (ortunately), d ys f (unction), ( x(%)

### D.5 pubmed\_abstracts

The susceptibilities for each head are shown in Figure 20. Below  $x$  stands for a token representing a number.

The positive susceptibilities for layer 0:

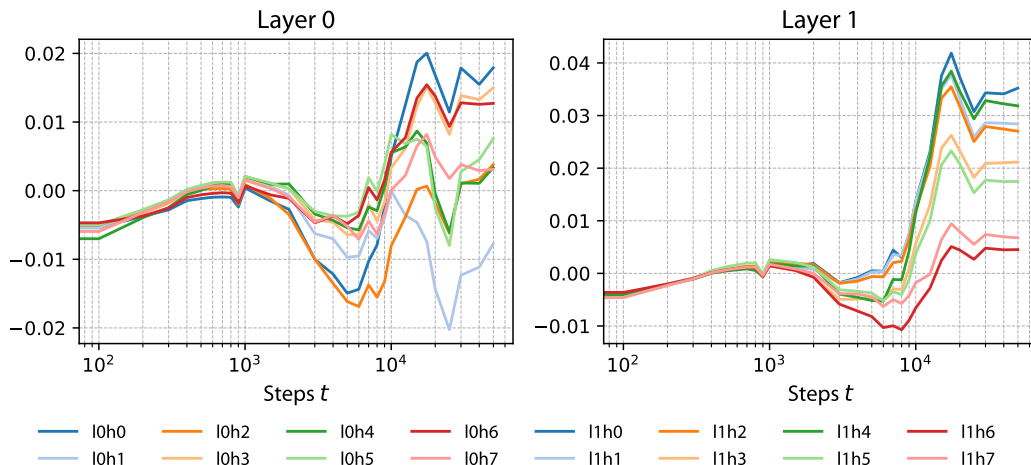


Figure 21: pubmed\_central susceptibilities for each head over training.

- 0:0: C a ++, ( x%), differe nces
- 0:1: differe nces, demon st ration, policy m akers
- 0:2: al cohol, differe nces, th y roid
- 0:3: ( x%), al cohol, differe nces
- 0:4: differe nces, poss ib ilities, demon st ration
- 0:5: ( x%), demon st ration, differe nces
- 0:6: al cohol, C a ++, ( x%)
- 0:7: C a ++, th y roid, al cohol

The positive susceptibilities for layer 1:

- 1:0: C a ++, ( x%), al cohol
- 1:1: C a ++, special token in chemical compound, wa vel ength
- 1:2: C a ++, al cohol, Th y roid
- 1:3: C a ++, al cohol, ( x%)
- 1:4: C a ++, th y roid, special token in chemical compound
- 1:5: C a ++, th y roid, al cohol
- 1:6: al cohol, anal ysis, special token
- 1:7: Un f ortunately, differe nces, k id ney

## D.6 pubmed\_central

The susceptibilities for each head are shown in Figure 21.

The positive susceptibilities for layer 0:

- 0:0: re f - type "=", ( x%), ://
- 0:1: ://, differe nces, al cohol
- 0:2: re f - type "=", ####, al cohol
- 0:3: ://, re f - type "=", ( x%)

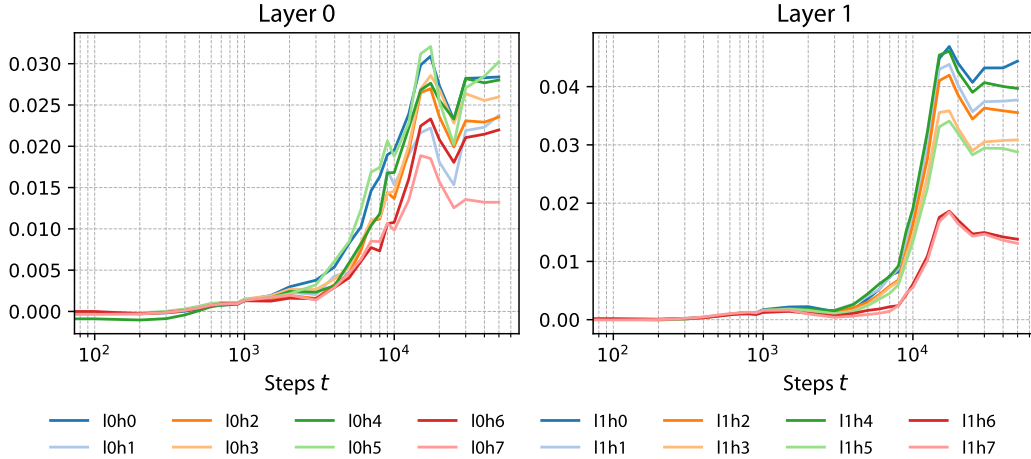


Figure 22: uspto\_backgrounds susceptibilities for each head over training.

- 0:4: (://), re f - type "=", special token
- 0:5: (://), re f - type "=", differe nces
- 0:6: re f - type "=", (://), full - l ength
- 0:7: (://), al cohol, full - l ength

The positive susceptibilities for layer 1:

- 1:0: re f - type "=", ( x%), (://)
- 1:1: re f - type "=", ( x%), special token
- 1:2: re f - type "=", (://), al cohol
- 1:3: re f - type "=", al cohol, ( x%)
- 1:4: re f - type "=", special token, b ibr (bibliography)
- 1:5: re f - type "=", special token, (://)
- 1:6: (://), al cohol, ch rom at ography
- 1:7: re f - type "=", (://), full - l ength

## D.7 uspto\_backgrounds

The susceptibilities for each head are shown in Figure 22.

The positive susceptibilities for layer 0:

- 0:0: wa vel ength, (://), special token
- 0:1: wa vel ength, (://), inst r uments
- 0:2: wa vel ength, es pecially, differe nces
- 0:3: wa vel ength, prot ocol, special token
- 0:4: wa vel ength, inst r uments, e ch oes
- 0:5: wa vel ength, at m osp here, effic i ency
- 0:6: wa vel ength, (://), inst r uments
- 0:7: wa vel ength, el im inate, inst r uments

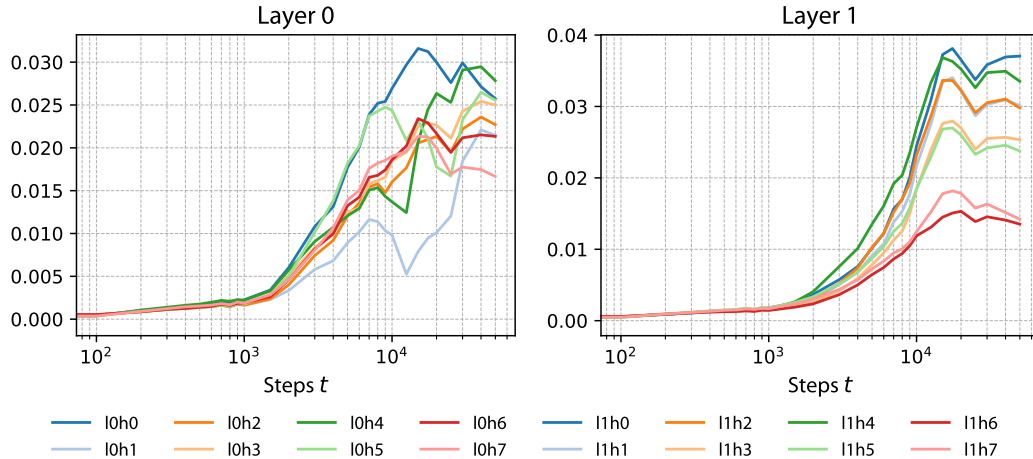


Figure 23: wikipedia\_en susceptibilities for each head over training.

The positive susceptibilities for layer 1:

- **1:0**: wa vel (ength), S od er (berg), t (oken)
- **1:1**: wa vel (ength), e ch (oes), S od er (berg)
- **1:2**: wa vel (ength), el im (inate), (arter) ial
- **1:3**: wa vel (ength), (arter) ial , special token
- **1:4**: wa vel (ength), mag n (itude), e ch (oes)
- **1:5**: wa vel (ength), e ch (oes), t (oken)
- **1:6**: wa vel (ength), S od er (berg), special token
- **1:7**: wa vel (ength), inst r (uments), Un f (ortunately)

## D.8 wikipedia\_en

The susceptibilities for each head are shown in Figure 23.

The positive susceptibilities for layer 0:

- **0:0**: (://), Ep (isode), al (bum)
- **0:1**: (://), al (bum), Ep (isode)
- **0:2**: al (bum), Ep (isode), (://)
- **0:3**: al (bum), (://), Ep (isode)
- **0:4**: al (bum), (://), differe (nces)
- **0:5**: (://), al (bum), R ef (erences)
- **0:6**: al (bum), (://), Ep (isode)
- **0:7**: al (bum), emb ro (idered), (://)

The positive susceptibilities for layer 1:

- **1:0**: P e (ople), (://), al (bum)
- **1:1**: Ep (isode), P e (ople), special token
- **1:2**: (://), R ef (erences), Ep (isode)

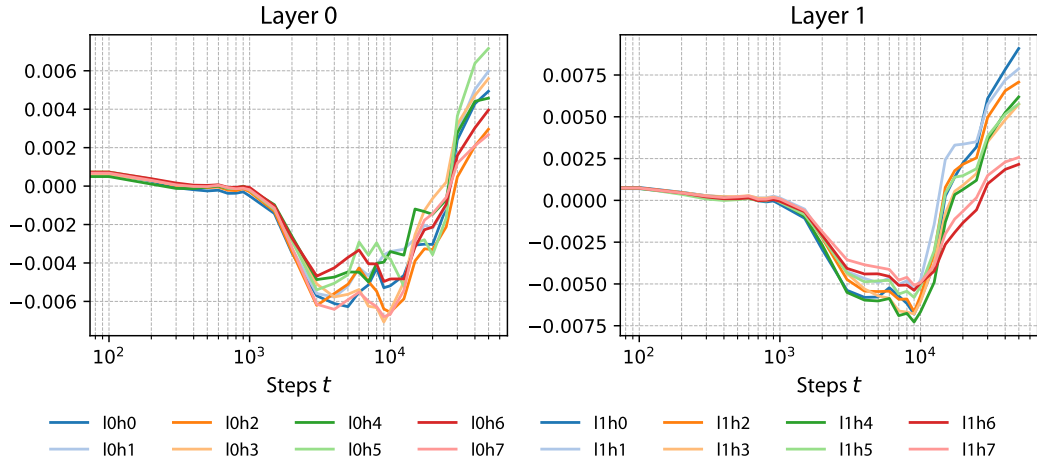


Figure 24: pile-cc susceptibilities for each head over training.

- 1:3: Char l (otten) b urg , Ep (isode) , ht (ml)
- 1:4: P e (ople) , al (bum) , R ef (erences)
- 1:5: P e (ople) , al (bum) , Char l (otten) b urg
- 1:6: al (bum) , P e (ople) , (://)
- 1:7: (://) , al (bum) , p it (chers)

**D.9 cc**

The susceptibilities for each head are shown in Figure 24. Instances of ":" typically occur as part of dictionaries, e.g. {" name ":"} but the preceding tokens vary.

The positive susceptibilities for layer 0:

- 0:0: ":", {, (://)
- 0:1: (://), ":", differe (nces)
- 0:2: ":", {" , ="
- 0:3: ":", {" , (://)
- 0:4: ":", (://), {"
- 0:5: (://), =" , max (imum)
- 0:6: ":", {" , ="
- 0:7: =" , ":" , P er (haps)

The positive susceptibilities for layer 1:

- 1:0: ":", =" , {"
- 1:1: ":", {" , ="
- 1:2: {" , =" , ":"
- 1:3: ":", {" , ="
- 1:4: {" , ":" , ="
- 1:5: {" , =" , (://)

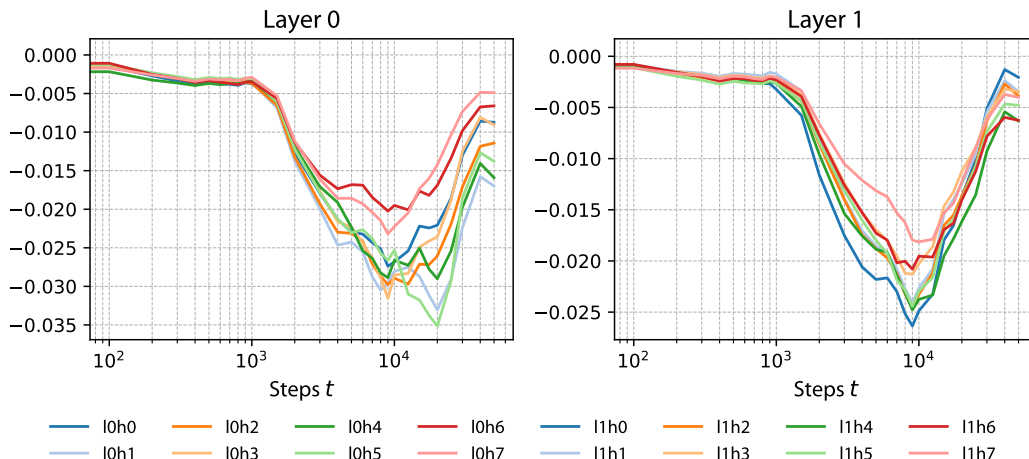


Figure 25: hackernews susceptibilities for each head over training.

- 1:6: {"", ":", "://"}
- 1:7: "=", ":", Un f `ortunately`

We note that the susceptibilities for heads on `cc` seem to be small, in some cases an order of magnitude smaller than the susceptibilities for other datasets. Note that by definition the susceptibility should be zero for a variation  $q \rightarrow q'$  where  $q'$  is distributed identically to  $q$ , so this could be because `cc` is a significant fraction of the Pile (18% according to Gao et al. (2020)). In Table 4 we give a variant of Table 1 where we compute the total positive and negative per-token susceptibility of 0:0 on the datasets `cc`, `github-all`.

Dataset	Total pos.	Total neg.	Sum	Scaled sum
<code>github-all</code>	167,995	-150,179	17,816	0.01
<code>cc</code>	129,467	-130,433	-966	-0.0006

Table 4: Total negative and positive per-token susceptibility for 0:0 on two datasets.

We note that the total positive and negative per-token susceptibilities are of a similar order of magnitude for both datasets, but their difference is an order of magnitude smaller (966 vs 17,816) and this explains the order of magnitude difference in the final susceptibility. Recall that macroscopic bodies have near zero electric charge because of the exact cancellation of very *large* amounts of positive and negative charge in physical matter at equilibrium; it seems a reasonable intuition that near zero susceptibilities are likewise caused by near-exact cancellations rather than both positive and negative per-token susceptibilities being small.

Also note that, given the similarity between the tokens with top positive susceptibility shown above, it is no surprise that Figure 24 shows little differentiation of the heads. This particular variation in the data distribution away from the full Pile is not enough to “break the symmetry” between the heads, by exposing them to distributions of patterns for which they have distinct preferences.

### D.10 hackernews

The susceptibilities for each head are shown in Figure 25.

The positive susceptibilities for layer 0:

- 0:0: C `++`, `://`, go `ogle`
- 0:1: `://`

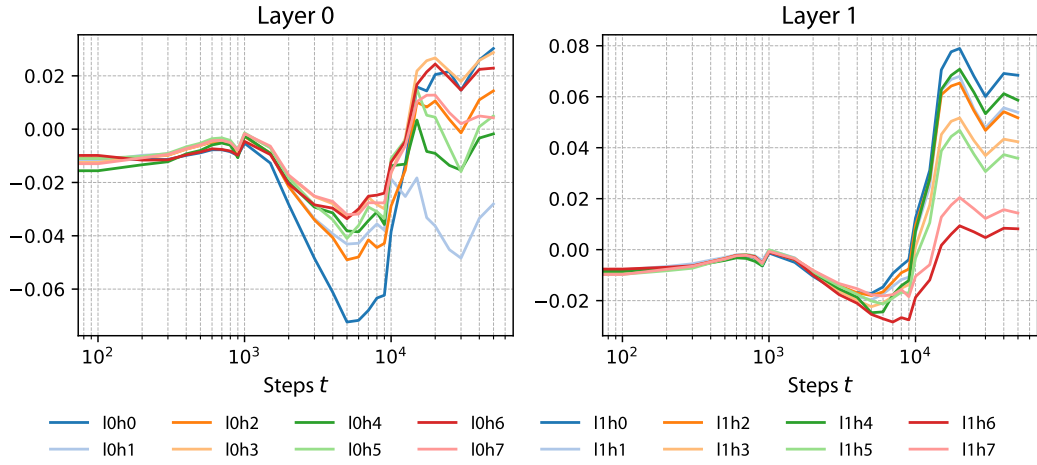


Figure 26: **github-all** susceptibilities for each head over training.

- 0:2: `://`, es `pecially`, `C ++`
- 0:3: `://`, `C ++`
- 0:4: `://`
- 0:5: `://`
- 0:6: `://`, `C ++`
- 0:7: `://`, `C ++`

The positive susceptibilities for layer 1:

- 1:0: `C ++`, go `ogle`, `://`
- 1:1: `://`, `C ++`, `Z uck er berg`
- 1:2: `://`, go `ogle`, `C ++`
- 1:3: `C ++`, go `ogle`, ht `ml`
- 1:4: `C ++`, `Z uck er berg`, go `ogle`
- 1:5: `C ++`, `://`, go `ogle`
- 1:6: `://`, go `ogle`, `Z uck er berg`
- 1:7: `://`, es `pecially`

Amusingly, 1:1 also has high susceptibility for `S od er berg` on `uspto_backgrounds`.

### D.11 github-all

The susceptibilities for each head are shown in Figure 26.

The positive susceptibilities for layer 0:

- 0:0: `"`, `()`, `>`
- 0:1: `"`, `://`, ht `ml`
- 0:2: `"`
- 0:3: `"`, `>`
- 0:4: `"`, `://`, ht `ml`

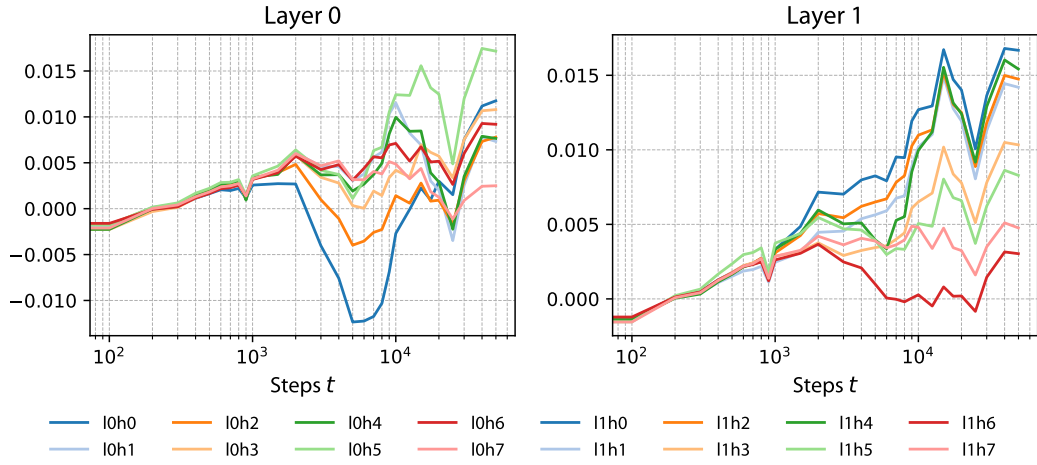


Figure 27: freeLAW susceptibilities for each head over training.

- 0:5: "=", ://
- 0:6: "="
- 0:7: "="

The positive susceptibilities for layer 1:

- 1:0: "="
- 1:1: "=", 1 length
- 1:2: "=", 1 length, ()
- 1:3: "="
- 1:4: "=", 1 length,
- 1:5: "=", ne xt ++, 1 length
- 1:6: "=", >, n um G l obal
- 1:7: "=", 1 length

For this dataset we see little variation in the top positive susceptibility tokens between heads, but there is a much wider variation when we look at *negative* susceptibilities.

The top negative susceptibilities for layer 1:

- 1:0: [ p for p in , con st base , ref et ched
- 1:1: host add r , <|endof|> , con st plan es
- 1:2: host add r , \_ in variable names , . en c ry pt , AP I
- 1:3: of , in , Qu at ro t
- 1:4: con st base , \_ in variable names , </
- 1:5: con st st d :: , To in variable names , im port or g .
- 1:6: < ul class , con st base , @ par am inv al id ate
- 1:7: <|endof|> , within HTML tags , role within HTML tags

## D.12 freelaw

The susceptibilities for each head are shown in Figure 27. Note ¶ is a common paragraph or section marker in legal documents and court opinions.

The positive susceptibilities for layer 0:

- 0:0: 0 d ys (sey), (://), differe (nces)
- 0:1: (://), differe (nces), demon st (ration)
- 0:2: 0 d ys (sey), (://), H ol (iday)
- 0:3: (://), inc ons ist (encies), H ol (iday)
- 0:4: (://), differe (nces), S up (reme)
- 0:5: (://), demon st (ration), S up (reme)
- 0:6: (://), 0 d ys (sey), S up (reme)
- 0:7: (://), 0 d ys (sey), P e (ople)

Here the 0 d ys (sey) in question is a shipwreck involved in a famous legal case between the United States, Spain and Peru and H ol (iday) is the name of a defendant in a murder case.

In layer 0 some examples of large negative susceptibilities include (defense) and the general pattern of dashes in wrapping words around lines such as rem (-) edy or A ri (-) z ona .

The positive susceptibilities for layer 1:

- 1:0: 0 d ys (sey), (://), d oc (uments)
- 1:1: d oc (uments), 0 d ys (sey), P e (ople)
- 1:2: (://), 0 d ys (sey), Miss iss (ipp) i
- 1:3: 0 d ys (sey), d oc (uments), P e (ople)
- 1:4: 0 d ys (sey), P e (ople), K ap n (icks)
- 1:5: 0 d ys (sey), P e (ople), d oc (uments)
- 1:6: 0 d ys (sey), (://), P e (ople)
- 1:7: (://), 0 d ys (sey), P e (ople)

Examples of high negative susceptibility tokens for layer 1 heads include (.) in abbreviations (e.g. C al (.) for California, the abbreviations of this kind of freelaw are very aggressive), (v) as in Birt v. Montgomery, and spaces and double spaces at the beginning of lines.

## D.13 philpapers

The susceptibilities for each head are shown in Figure 28.

The positive susceptibilities for layer 0:

- 0:0: (://), differe (nces), G ( ) space following a mathematical object
- 0:1: differe (nces), (://), resear (cher)
- 0:2: K ier ke (ga) rd, unfam (iliar), differe (nces)
- 0:3: (://), special token, differe (nces)
- 0:4: (://), differe (nces), poss ib (ilities)
- 0:5: (://), differe (nces), special token

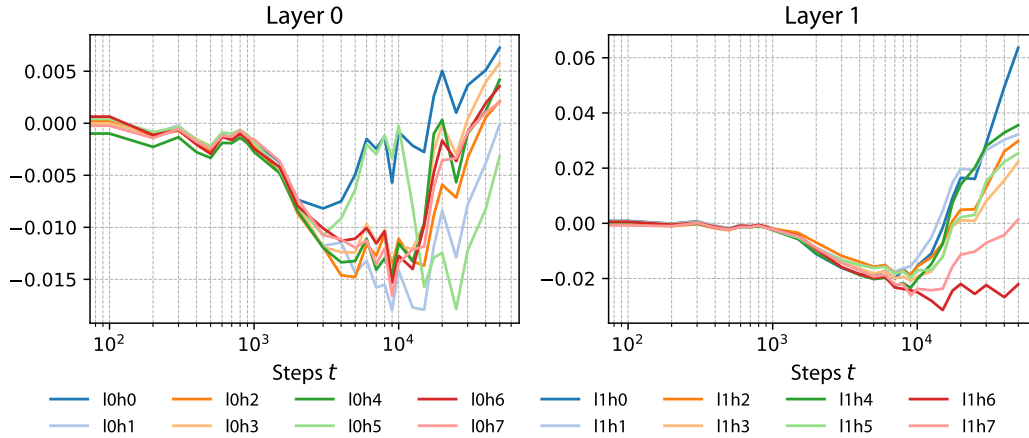


Figure 28: philpapers susceptibilities for each head over training.

- **0:6**: `://`, special token, `differe nces`
- **0:7**: `://`, `K ier ke ga rd , unfam iliar`

In layer 0 some examples of large negative susceptibilities are `is` and `does` following single letter variable names, as in “*p* does not guarantee”.

The positive susceptibilities for layer 1:

- **1:0**: special tokens
- **1:1**: special token, `K ier ke ga rd , special token`
- **1:2**: special token, `K ier ke ga rd , special token`
- **1:3**: special token, `K ier ke ga rd , special token`
- **1:4**: special token, `K ier ke ga rd , special token`
- **1:5**: special token, `K ier ke ga rd , special token`
- **1:6**: `://`, special tokens
- **1:7**: `://`, `pr inc iple , poss ib ilities`

As for `freelaw` we see high negative susceptibility in layer 1 heads for `.` in abbreviations. We also see letters used for enumeration e.g. 2011 `a`.

#### D.14 stackexchange

The susceptibilities for each head are shown in Figure 29.

The positive susceptibilities for layer 0:

- **0:0**: `=`, `()`, `L ength` as part of function name
- **0:1**: `://`, `=`, `hop ef ully`
- **0:2**: `://`, `=`, `->`
- **0:3**: `://`, `=`, `>`
- **0:4**: `://`, `=`, `differe nces`
- **0:5**: `://`, `=`, special token
- **0:6**: `=`, `://`, `>`

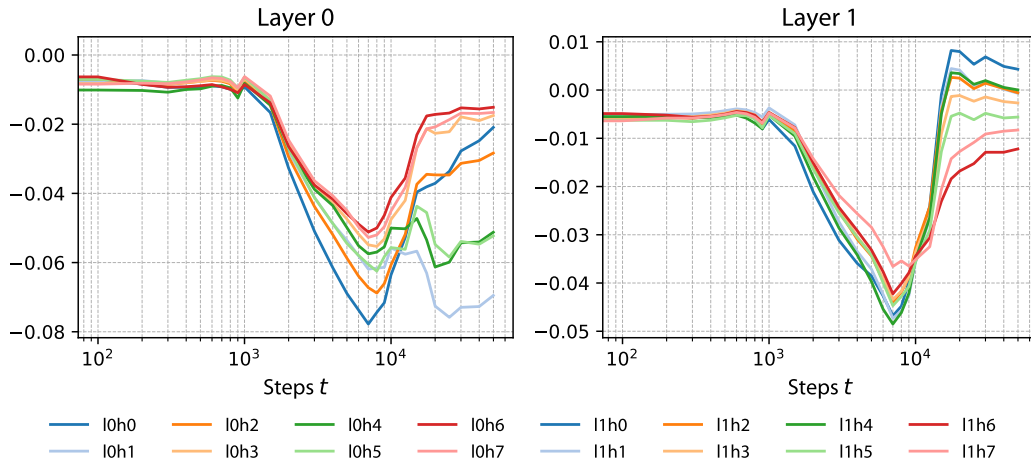


Figure 29: stackexchange susceptibilities for each head over training.

- **0:7**: "=", "://", >

High negative susceptibility tokens for layer 0 heads include `with`, `where`, `in`, `Having`.

The positive susceptibilities for layer 1:

- **1:0**: ":", "=", ()
- **1:1**: ":", "=", >
- **1:2**: ":", "=", ()
- **1:3**: "=", ":", >
- **1:4**: "=", (), ":", "
- **1:5**: "=", (), ":", "
- **1:6**: "://", special token, "=", "
- **1:7**: "=", "://", Un f `ortunately`

High negative susceptibility tokens include `in`, `with` and `/` used to separate two items (e.g. add/remove), also `,`, `;`

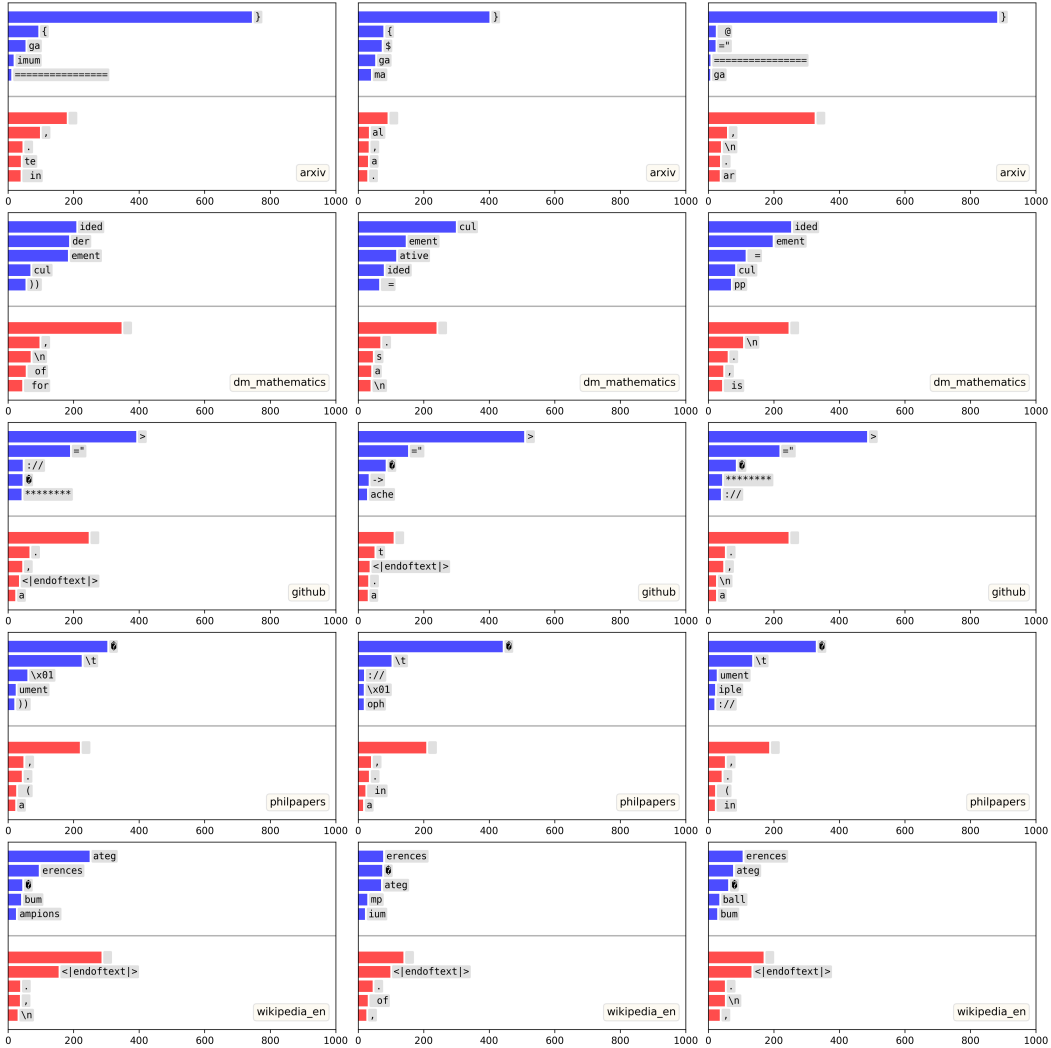


Figure 30: Token occurrences in top 1,000 positive (blue) and negative (red) per-token susceptibilities across three heads fixed across columns (left to right: [0:0](#), [1:2](#), [1:7](#)) for five different datasets fixed across rows.

## E Top $k$ per-token susceptibilities

In Figure 30, we take 160 random samples from each of five datasets (arxiv, dm\_mathematics, github, philpapers, wikipedia\_en) and count the number of occurrences of tokens in the top 1000 most positive and most negative susceptibilities for a given head and dataset. We observe that both the frequency and ordering of most frequent tokens changes for each of the three heads [0:0](#), [1:2](#), [1:7](#).

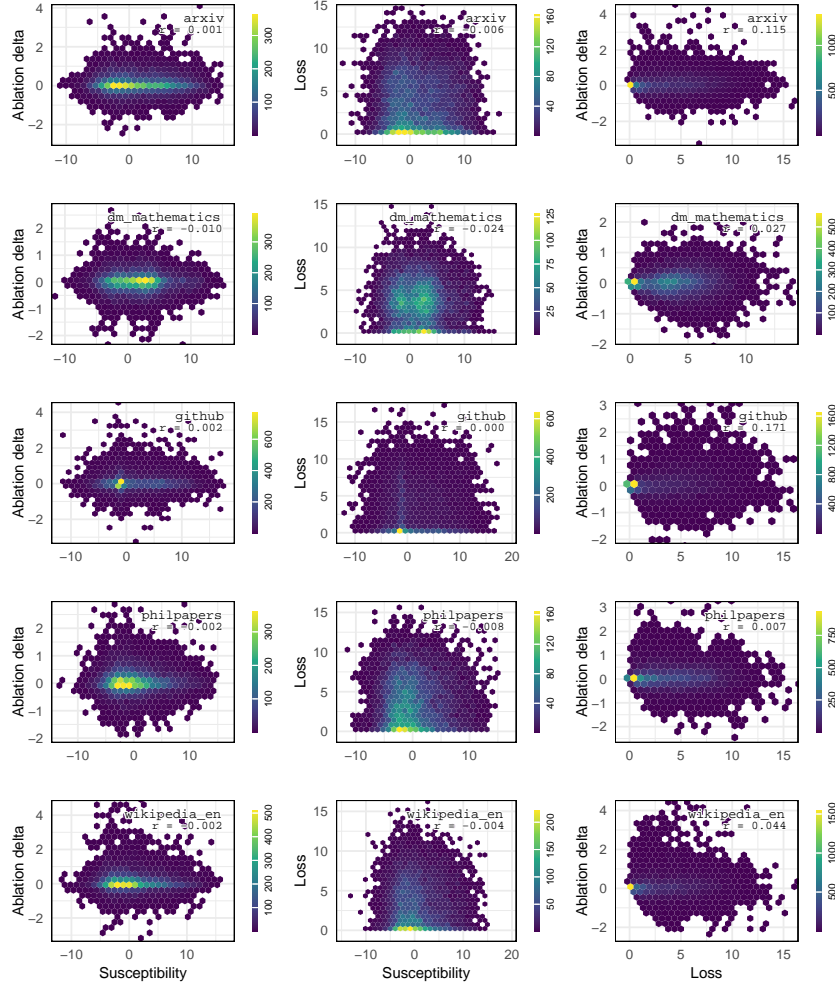


Figure 31: Pairwise comparisons of per-token susceptibilities, ablation, and loss as density maps for attention head 0:0. The color bar legend on the right of each subplot indicates the number of points represented by each colored hex.

## F Per-token Metric Comparisons

In Figure 31 we compare the per-token susceptibility values against per-token zero-ablation loss differences and original loss values for each of the same tokens using head 0:0. Figure 31 and Figure 7 use 10k tokens randomly sampled from 160 contexts, themselves randomly sampled from their respective datasets.

We see several distinct patterns for different datasets reflecting their differences. We also note that the information offered by each of these metrics appears to be uncorrelated with each other, demonstrating that the susceptibility is measuring its own distinct signal.

In Figure 32, we see a specific example where the induction pattern is particularly visible in the positive susceptibilities, while there is no discernible induction pattern in the zero-ablation loss differences or original per-token loss.

## G Per-token Susceptibility Variation with Context

In Figure 33 we plot the change in average per-token susceptibility for each attention head using 160 contexts from each of the following datasets: pile1m, arxiv, dm\_mathematics, enron\_emails,



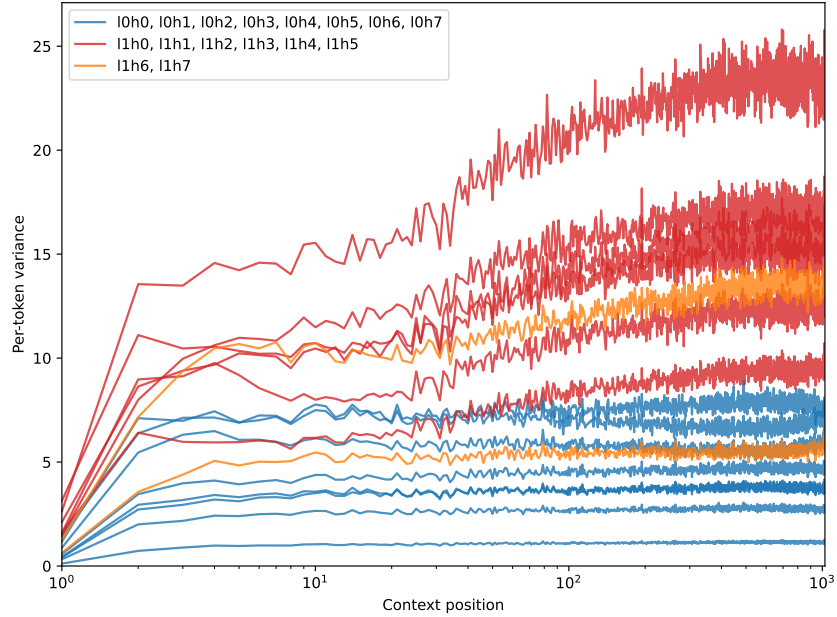


Figure 34: **Per-token susceptibility variance as a function of context length.** The variance in per-token susceptibilities over pairs  $x, y$  where  $x$  has a given length. Layer 0 heads are shown in blue, layer 1 induction heads in orange and the other layer 1 heads in red.

freelaw, github, nih\_exporter, philpapers, pubmed\_abstracts, pubmed\_central, stackexchange, uspto\_backgrounds, wikipedia\_en.

In Section 4.4 we noted an interesting variation of the per-token susceptibilities with context length, with the layer 1 heads (1:0-1:5) showing a strong increase as a function of length. In Figure 34 we additionally show the variance of the same measurements, for the same datasets.

In general layer 1 heads (with the exception of one of the induction heads) have significantly higher variance in the per-token susceptibilities. We interpret this as another indication of layer 1 heads performing more nontrivial, context-dependent, computations.

### G.1 Explaining Susceptibility Differences

In Figure 35 we provide some additional information on the distribution of susceptibility values for the space token for two heads in the context of Section 4.5.

### G.2 Bimodal Tokens

In this section we collect additional data relevant to the discussion in Section 4.6. In Figure 36 we show the distribution of susceptibilities for (1:7) and the token / in enron\_emails.

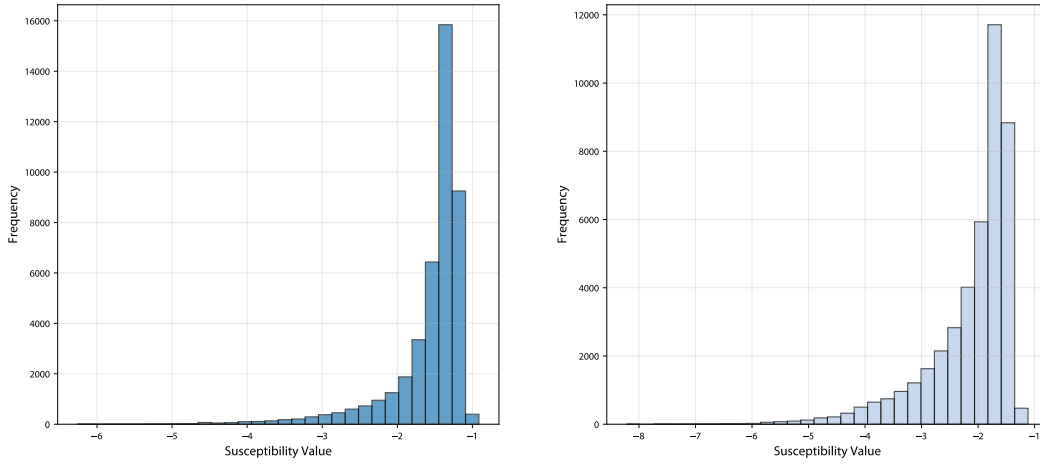


Figure 35: **Histogram of susceptibilities.** Shown is a histogram of per-token susceptibility values for the space token  across 163k tokens sampled from `github-all`. *Left:* `0:0`, *Right:* `0:1`.

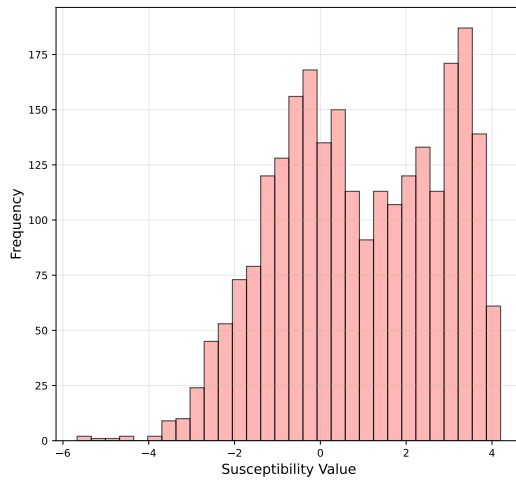


Figure 36: **Bimodal token.** Histograms showing frequency of certain susceptibility values for `1:7` and token `/` in `enron_emails`.